

GROWTH AND CHARACTERIZATION OF BORON DOPED β C-SIC AS SOLAR CELL MATERIAL

September 16, 2014

PHILIPP SCHUH
MASTER'S THESIS



Linköping University

FAU FRIEDRICH-ALEXANDER
UNIVERSITÄT
ERLANGEN-NÜRNBERG

Supervisors:

Prof. Dr.-Ing. P. Wellmann (University of Erlangen-Nuremberg)
Dr. M. Syväjärvi (University of Linköping)

ABSTRACT

Highly boron doped ($> 10^{18} \frac{1}{\text{cm}^3}$) 3C-SiC layers were grown using the sublimation epitaxy approach. The cubic seeding material was grown on 4° off-axis 4H-SiC substrates at different growth rates. Afterwards the as-grown crystals were characterized in terms of morphology (DPBs and SFs), inclusions (4H-SiC and 6H-SiC) and optical properties (LTPL and RTPL). The growth of the boron doped layers was performed at the same ramp-up ($\frac{20\text{K}}{\text{min}}$) and the same growth temperature (1850°C) with a source material from Erlangen (doping concentration of $3 \cdot 10^{18} \frac{1}{\text{cm}^3}$). The varying factor was the pressure. However, due to a lack of time the results in the pressure setups are not compared and only the one with the highest expected mean-free-path and therefore the highest boron concentration was evaluated. The PL measurements showed a DAP peak in the range of 950nm to 1400nm.

ACKNOWLEDGEMENTS

First of all, I would like to thank my supervisors Prof. Dr.-Ing. P. Wellmann (University of Erlangen-Nuremberg) and Dr. M. Syväjärvi (University of Linköping) for giving me the possibility to contribute to the research of silicon carbide in Linköping, Sweden. Furthermore, I thank them for all their personal and scientific support during my work on this thesis.

Special thanks to M. Sc. Valdas Jokubavicius for introducing me to all the equipment and withstanding my persistent questioning of the field. Moreover, I thank him for his scientific support and the declaring talks in the lab.

Fang Wei Chen for helping with the growth runs for the seeding material and sharing her results. Also I would like to thank the whole semiconductor team at LIU for their warm welcome and their help concerning interpretations, measurements and/or discussions about results.

Dipl.-Ing. Martin Wilhelm and Simon Johannes Kinkelein for Raman and PL measurements as well as interpretations of the results, which helped me a lot during my work.

At last I would like to thank the German Association for Crystal Growth and the ERASMUS exchange program for their financial support.

CONTENTS

i INTRODUCTION	1
ii GENERAL ASPECTS	5
1 OPPORTUNITIES OF 3C-SIC IN THE PHOTOVOLTAIC	7
2 SUBLIMATION EPITAXY OF 3C-SIC	11
3 DOPING OF 3C-SIC IN SUBLIMATION EPITAXY	21
4 DEFECTS IN SIC	23
iii EXPERIMENTAL	25
5 HETEROEPITAXIAL GROWTH OF 3C-SIC	27
6 HOMOEPITAXIAL GROWTH OF BORON DOPED 3C-SIC	31
iv RESULTS AND DISCUSSION	33
7 GROWTH CONDITIONS FOR THE 3C-SIC SEEDS	35
8 MORPHOLOGY AND DEFECTS IN 3C-SIC SEEDS	39
9 PL-, RAMAN AND CL-MEASUREMENTS OF THE SEED- ING MATERIAL	45
10 GROWTH RATE FOR BORON DOPED HOMOEPITAX- IAL LAYER	55
11 PL-MEASUREMENT OF DOPED SAMPLES	59
v CONCLUSION	63
12 CONCLUSION	65
BIBLIOGRAPHY	67

Part I

INTRODUCTION

INTRODUCTION

Conventional solar cells have an efficiency limited by the Shockley Queisser (SQ) model, considering the losses by blackbody radiation, radiative recombination and spectral misfits [61]. However, the SQ limit of approximately 30% efficiency can be broken by either (i) tandem solar cells or by (ii) intermediate band solar cells (IBSCs). A tandem solar cell stacks different semiconducting materials with decreasing (top to bottom) bandgaps (E_G), to absorb a larger spectral area of incoming light [6]. Thus, a higher efficiency can be achieved. This method adds up the efficiencies of different pn-junctions. For IBSCs an IB is introduced between the conduction band (CB) and the valence band (VB), leading to an additional absorption of lower energetic photons and therefore broadening the spectral yield. The highest efficiency for tandem solar cells is 55.4%, which is below the 63.1% in IBSCs [1]. The reason for the poorer performance of tandem cells is the need for at least two photons (depending on the architecture) to deliver an electron to the external circuit. This leads to a quantum efficiency of $\frac{1}{2}$, whereas for IBSCs only the lower energetic photons inducing an electron into the IB need a second photon. The higher energetic photons deliver an electron directly into the external circuit. Hence, the quantum efficiency of IBSCs is above $\frac{1}{2}$ and can be compared to a triple cell [1].

Boron doped cubic silicon carbide (β C-SiC) could be a very promising host material for the fabrication of intermediate band (IB) solar cells with a theoretical efficiency of up to 63.1% [1, 2]. However, such a solar cell concept has not yet been explored for β C-SiC due to a lack of high quality material.

The applicability of boron doped β C-SiC in impurity photovoltaic (IP) solar cells was initially explored by Richards et al. [6]. Some advantages which make SiC the material of choice are the availability of silicon (Si) and carbon (C), as well as the non-toxic behaviour. For the production of electrical applications a passivation of SiC can easily be accomplished by growing silicon dioxide (SiO_2). Moreover SiC exhibits excellent electrical properties, which are shown in [29] (Table 2.1). Regarding the

β C-SiC, the electrical properties describe a high isotropic electron mobility of up to $1000 \frac{\text{cm}^2}{\text{V}\cdot\text{s}}$ and the lowest E_G of the commonly used polytypes, of 2.39eV [20]. Luque et al. calculated the maximum achievable efficiency of IBSCs with the corresponding bandgaps lying between 1.93eV and 2.14eV [1]. More balanced calculations were made by Beaucarne et. al, resulting a broad maximum of 2.0eV to 2.5eV [20]. This makes β C-SiC very attractive for this kind of solar cell concept, as it fits to this maximum value of efficiency for the third generation photovoltaics.

Chemical vapor deposition (CVD) and physical vapor transport (PVT) are the most common techniques used to produce high quality SiC. Other techniques and modifications can be found in [29]. The fabrication of high quality β C-SiC is still in research phase, whereas other polytypes like 4H-SiC and 6H-SiC are already available on the market. Richards et al. already tried to produce IBSCs using β C-SiC doped by ion-implantation, but a photocurrent could not be observed by the reason of low quality material [6]. Using sublimation epitaxy, it is possible to produce high quality, thick β C-SiC layers (up to 1mm) by using off-axis 6H-SiC substrates [34, 36, 43, 44, 45].

In this thesis the growth of boron doped β C-SiC on off-axis hexagonal SiC substrates is explored. The work is divided into several interconnected chapters. The first part describes the stabilization of nominally undoped β C-SiC on off-axis substrates. In the next part, the growth of boron doped β C-SiC layers is discussed. In the end, an analysis of the structural and optical properties of the as-grown layers is examined.

Part II

GENERAL ASPECTS

OPPORTUNITIES OF 3C-SiC IN THE PHOTOVOLTAIC

THE PRINCIPLE OF INTERMEDIATE BAND SOLAR CELLS

A conventional solar cell is based on the direct excitation of an electron from the valence band into the conduction band of a semiconductor. By introducing an intermediate band the concept of the intermediate band solar cell (IBSC) is generated. Figure 1 shows the basic structure of an IBSC pn-junction and a possible bandgap diagram for it.

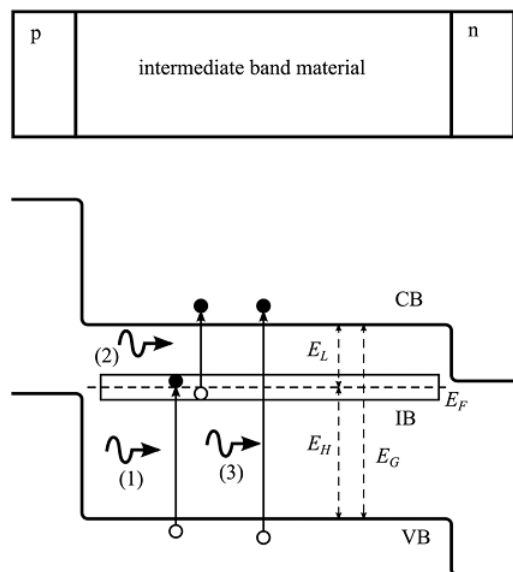


Figure 1: Structure of an intermediate band solar cell (IBSC), and a simplified bandgap diagram, as well as the three possible photon absorption processes [2].

With this additional intermediate band in the bandgap it is possible to absorb photons with energies (E_H) lower than the bandgap and excite electrons into the IB (1). In this state another photon of lower energies (E_L) can excite the electron into the CB (2). This two-step process adds up to the efficiency given by process (3), resulting in a quantum efficiency between $\frac{1}{2}$ and 2 (fig.1)[1].

The increase of the photocurrent, based on the intermediate photovoltaic (IPV) effect can be calculated by equation 1 [20].

$$I_{L,IPV}(\Delta E_F) = q \int_0^W [-U(x, \Delta E_F)] dx \quad (1)$$

This equation is based on a model presented by Keevers and Green, describing a solar cell with a nonmidgap, but deep impurity level (Fig. 2) [31]. The model itself is based on a superposition approach, assuming constant quasi Fermi-levels (ΔE_F) through the whole device (represented in fig. 2 as ϵ_{FC} , ϵ_{FI} and ϵ_{FV}) [20, 31]. This also leads to infinite carrier mobilities [20, 1]. The photocurrent ($I_{L,IPV}$) can be calculated by multiplying the electron charge (q) with the integral of the negative recombination rate (U) over the thickness (W) of the solar cell. In case of a generation domination due to the IPV effect the recombination rate will be negative.

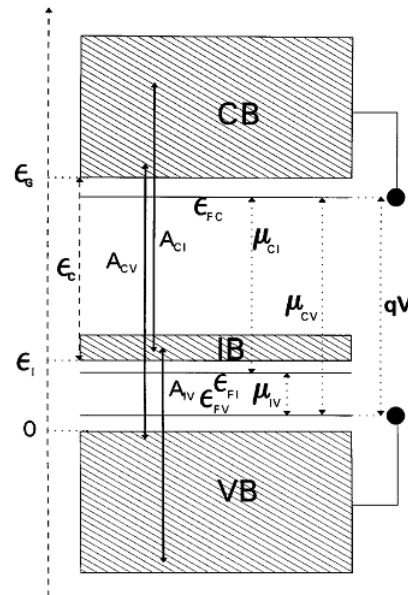


Figure 2: Band diagram of an intermediate band solar cell, featuring a nonmidgap, deep impurity level [1].

The overall current I between the CB, the IB and the VB can be calculated by equation 2 [1].

$$\frac{I}{q} = [\dot{N}(\epsilon_G, T_S, \infty, 0) - \dot{N}(\epsilon_G, T_a, \infty, \mu_{CV})] + [\dot{N}(\epsilon_C, \epsilon_G, T_S, 0) - \dot{N}(\epsilon_C, \epsilon_G, T_a, \mu_{CI})] \quad (2)$$

The function \dot{N} describes the flux of photons leaving the semiconductor depending on the energy differences of the quasi fermilevels (ϵ_G and ϵ_C), the temperature of the system (T_S for the solar temperature and T_a for crystalline network temperature) and the chemical potential (μ) [1]. Actually, there is no current extracted from the IB. Therefore, the first term of the equation 2 describes the current of photons exciting an electron from the VB to the CB. The second term describes the current of photons exciting an electron from the IB to the CB. The applied energy levels can be seen in figure 2. The deviation of equation 2, as well as the calculation for the chemical potentials can be found in [1].

Additionally, to the total current the actual I-V curve and the power delivered current and voltage can be calculated using equation 2. Using the featuring maximum of this curve and dividing it by the power provided by concentrated sunlight on the illuminated solar cell leads to the total efficiency of the device [1]. Figure 3 is showing a plot of the theoretically achievable efficiency over the energy for different solar cell concepts.

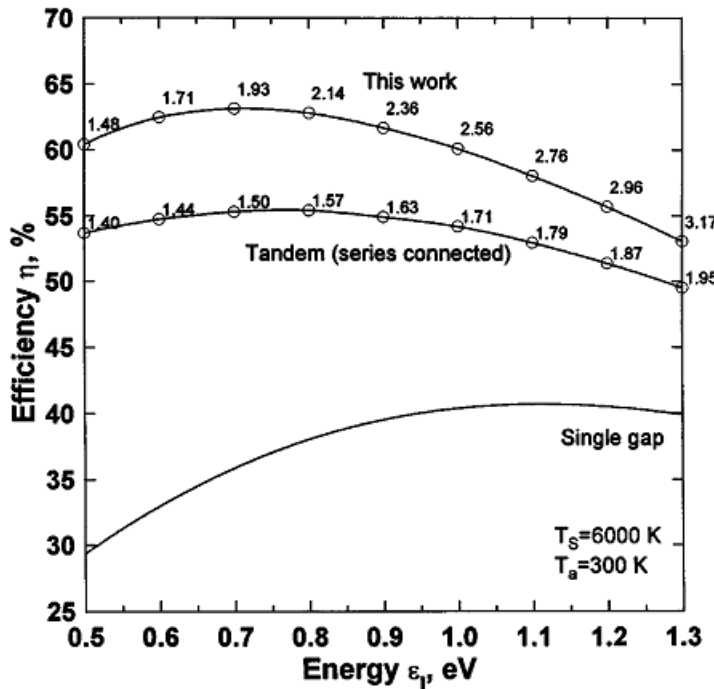


Figure 3: Efficiency over the Energy ϵ_I with the corresponding bandgaps, simulated using the Shokley-Queisser model, for single gap, tandem and intermediate band solar cells [1].

For the calculation of the curve marked as "This work" equation 2 was used, inserting a constant position of the IB (constant ϵ_I) and varying the bandgap (ϵ_G). The deviation and the formula for the simulation of the tandem cell can be reviewed in [1]. Luque's work shows a theoretical efficiency of 63,1% for IBSCs compared to 40,7% for tandem solar cells. However, these numbers have to be treated with caution, as this model was calculated under boundary conditions for a perfect solar cell.

OPTIMIZATION OF IBSCS

Since the theory of IBSCs was proposed in the year 1997 [1], the knowledge in this subject became more established and different opportunities for optimizing this concept came up. Some of those possibilities, including transitions between the IB, the VB and the CB, are stated in the work of A. Marti et al. [2].

In fact, a good engineering of the absorption coefficients has to be achieved, to minimize the thermal loss due to higher energetic photons. Moreover, a prevention of the nonradiative recombination would be desirable. Hence, a delocalized wavefunction of the electrons could be a potential solution as described in [2].

3C-SiC AS A MATERIAL FOR IBSCS

The concept of IBSCs can only work for semiconductors, featuring a bandgap between 1.9eV and 2.5eV [20, 1, 6], such as silicon carbide. Especially the cubic polytype of SiC exhibiting an indirect bandgap of 2.2eV seems to be a promising material [20, 6]. Recent experiments were using the model of a deep impurity level, locating the dopant energy at one third above the VB (0.6eV - 0.8eV) or below the CB by doping with boron [6, 20]. Although a theoretical efficiency of 63.1% for a perfect IBSC can be achieved (Fig. 3), the efficiency for a realistic SiC IBSC lies around 38% for a 100% radiative efficient impurity level [6, 20].

2

SUBLIMATION EPITAXY OF β C-SiC

The sublimation epitaxy is a modification of the physical vapor transport (PVT) technique [47, 12]. A vertical reactor, as shown in fig. 4, is heated up to a temperature around 2000°C and a temperature gradient from source to substrate is established due to the geometry of the growth cell [47, 12]. The source material is always placed in the higher temperature zone compared to the substrate material. Thus, the source material sublimes and due to the temperature gradient between the source and the substrate, gas species of Si, Si₂C and SiC₂ are transported to the surface of the substrate and recrystallise [47].

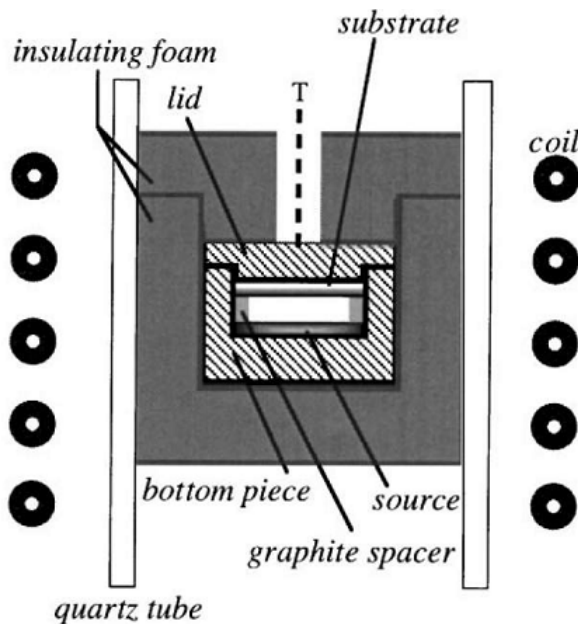


Figure 4: Setup for the sublimation epitaxy, including the heating coils, the quartz tube with the insulation foam and the actual crucible in the inner part [35].

The heating is realised by water cooled copper made induction coils, wrapped around a quartz tube. The temperature is measured on top of the crucible using an optical pyrometer. A direct measurement of the temperature inside the container is not possible by this setup. However, a temperature profile of the growing chamber can be simulated numerically [44]. The pressure

in the quartz tube is $10^{-4} - 10^{-5}$ mbar during the whole growth process [44]. For the insulating material, a cylindric foam made of porous graphite layers is used to avoid dissipation of heat from the graphite container, in which the growth of 3C-SiC is established.

Inside the graphite container the materials are stacked in a sandwich-like arrangement (fig. 4). The distance between source and substrate can vary between 0.2mm and 3mm [47, 63]. A distance of 1mm is used in sublimation epitaxy to avoid a reaction of the sublimed gas species with the crucible wall and to provide a direct mass transport from source to substrate [53]. The growth rate can vary from $100 \frac{\mu\text{m}}{\text{h}}$ to $800 \frac{\mu\text{m}}{\text{h}}$ [53].

From the bottom to the top the first object in the sandwich-like arrangement is a tantalum foil (not shown in fig. 4) with the thickness of approximately $500 \mu\text{m}$. Tantalum reacts with carbon at elevated temperatures and forms tantalum carbide (TaC), hence the foil works as a carbon getter to control the $\frac{\text{Si}}{\text{C}}$ ratio and to prevent a graphitization of the source [51, 47, 35, 21]. One tantalum foil can be used several times but the $\frac{\text{Si}}{\text{C}}$ ratio will probably change. However, this effect can influence the incorporation of boron [35]. The source is placed on top of the foil, which is a polycrystalline material, different from the PVT process where SiC powder is sublimed. Therefore no inhomogeneities in density or surface roughness are expected from this source, leading to a homogeneous sublimation [53]. Above the source a 1mm thick graphite spacer with a $10 \times 10 \text{ mm}^2$ opening is placed. The substrate lies on top of this opening. To prevent a back-side sublimation of the substrate a graphite plate is put above (not shown in fig. 4).

There are two possibilities to introduce doping species into the growth process: (i) Via gasphase or (ii) via co-doping from the source. For gases like nitrogen (N_2) or argon (Ar), the walls are permeable [47]. Hence, the doping concentration can be controlled by the gas-inlet and the adjusted pressure in the quartz tube [51]. The second approach is based on the usage of a doped source material (e.g. boron doped, polycrystalline SiC) or a doped substrate [51, 32].

GROWTH MECHANICS OF 3C-SiC

The formation of 3C-SiC on off-axis surfaces overcomes two stages. The first one is the creation of 2D nuclei of 3C-SiC on the substrate step terraces. The second is the lateral enlargement of those nuclei along the step-flow direction. Figure 5 shows three different possible attaching points on the surface of a terrace. The position "C" describes the weakest attaching point, featuring only one bonding site at the bottom of the atom. Position "B" features two and position "A" features three attaching points. Therefore position "A" is thermodynamically and energetically favored to attach an atom.

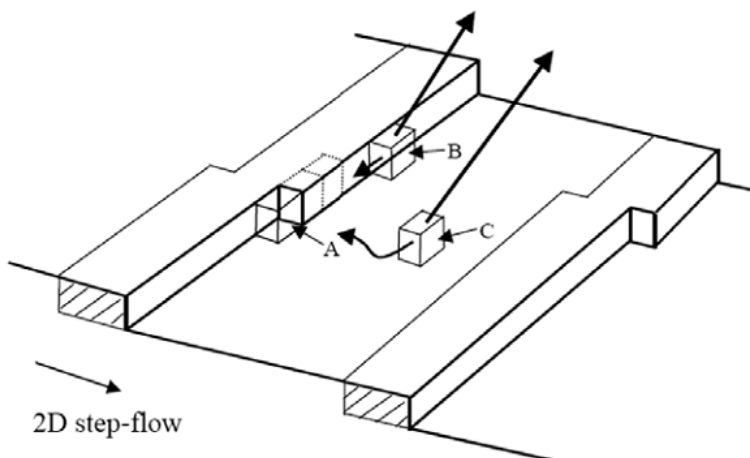


Figure 5: Schematic model of the lateral enlargement in step-flow direction, including different attaching points and the 2D step-flow direction [8].

Adatoms will diffuse on the surface until they find kinks or step-edges where they are incorporated into the lattice sites. This growth can be described as a homoepitaxial growth process without a change of the polytype. If they do not reach the kink sites a 2D nuclei of 3C-SiC is formed in the middle of a terrace (Fig. 5). Therefore, the larger the terrace, the higher the probability to create a 2D island of 3C-SiC at the same growth conditions [44].

The initial 2D nucleation on terraces is followed by a lateral enlargement in step-flow direction [9]. Those two different mechanisms are regarded closer in this chapter, also considering the different sorptions on a stepped surface (Fig. 6).

Figure 6 features a schematic model of a stepped surface, which evolve during a growth process (e.g. off-axis 4H-SiC or 6H-SiC

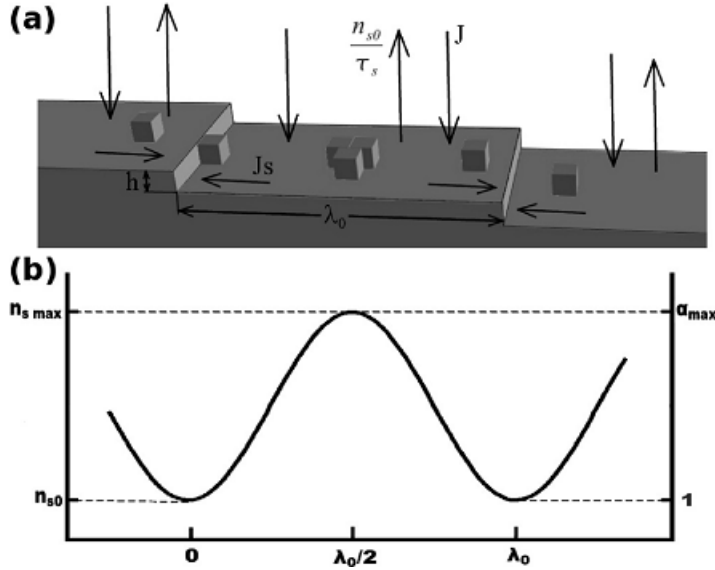


Figure 6: (a) Schematic model of a stepped surface with the different sorption processes and (b) the distribution of adatom concentration and supersaturation ratio on a stepped surface [44].

substrates) [44, 9, 58, 45, 36]. The top picture (fig 6 a) shows the absorption flux J , the desorption flux $\frac{n_{s0}}{\tau_s}$ (n_0 equals the density of absorption sites on the surface and τ_s equals the surface diffusion length), the surface flux I_s , the step-height h and the step-length λ_0 . The maximum supersaturation can be calculated by [44]

$$\alpha_{\max} = 1 + \frac{\lambda_0 n_0 R \tau_s}{2 \lambda_s h n_{s0}} \cdot \tanh \left(\frac{\lambda_0}{4 \lambda_s} \right) \quad (3)$$

where R is the growth rate. With this equation the highest supersaturation can be located in the middle of a terrace.

A critical value for the supersaturation leads to a nucleation of two-dimensional disk shaped nuclei and can be calculated with [44]

$$\alpha_{\text{crit}} = \exp \left(\frac{\pi h \sigma^2 \Omega}{(65 - \ln(10^{12})) k_b^2 T^2} \right) \quad (4)$$

where σ is the surface free energy of the substrate and Ω is the volume of the SiC pair [44]. Those two-dimensional shaped nuclei are initial stage of 3C-SiC formation. Therefore the critical

supersaturation should be maintained during the growth process.

It was shown that the growth of hexagonal SiC in sublimation epitaxy is favored at lower temperatures (approximately 1700°C – 1800°C) and lower supersaturation (due to step-flow growth), whereas cubic SiC starts to form at high supersaturation and on flat terraces [44, 9].

The dependence of the growth rate on the temperature and the pressure were observed by Hupfer et al. [54]. In this work a theoretical model for the mean free path (MFP) was calculated, describing the mass transport from source to substrate. In this calculation, the Sutherland model was included depicting the molecular forces (equation 5) [54, 52].

$$\lambda = \frac{k_B T}{\sqrt{2} \sigma p} \text{ with } \sigma = \pi(r_1 + r_2)^2 \text{ and } r = r_\infty \sqrt{1 + \frac{T_V}{T}} \quad (5)$$

In equation 5, λ represents the mean free path, σ (collision cross section) introduces the dependency between the molecular radius (r_1 and r_2), which is described by the sutherland parameters r_∞ and T_V [54]. The corresponding material values for the main gases during the SiC growth process (Si, Si₂C and SiC₂) were calculated using the diffusion coefficient [54]. By the assumption of high dilution of the gas species in the growth chamber and an interaction with just the inert-gas, the MFP for each species was calculated. Figure 7 shows the MFP for Si in Ar atmosphere and the percentage of unscattered particles over the temperature and pressure. It shows that almost no sublimed particles reach the substrate at high pressure (2). However, if the MFP is at least in the range of the distance between source and substrate (1mm), there is almost no interaction between the gas species (point (1) in picture 7).

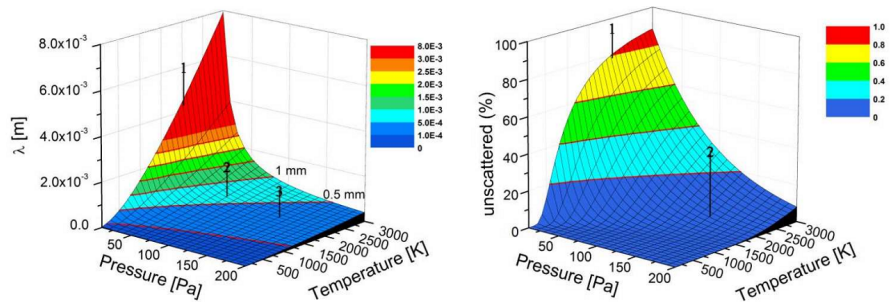


Figure 7: The calculated MFP for Si in Ar atmosphere versus temperature and pressure (left side) and the percentage of unscattered Si species versus temperature and pressure (right side)[54].

In case number 2 (fig. 7) the mass transport is limited by the pressure and occurs by diffusion, whereas in case number 1 (fig. 7) ballistic mass transport occurs [54]. Hence, a high growth rate can be maintained despite high pressure, if the MFP is long enough.

3C-SiC GROWTH ON OFF-ORIENTED SUBSTRATES USING SUBLIMATION EPITAXY

To achieve a decent lateral enlargement, substrates with an off-axis angle have to be used. The substrates used in this thesis are 4° off-axis 4H-SiC substrates with the step-flow direction and the off-orientation direction facing $[11\bar{2}0]$. Those substrates feature terrace widths of around 200nm and step heights of around 10nm [9].

A model for the growth of cubic SiC on 4° off-axis was proposed in the thesis of P. Chen [9]. Introducing those off-axis substrates, featuring steps from the beginning, is the point of matter in growing high quality bulk like 3C-SiC.

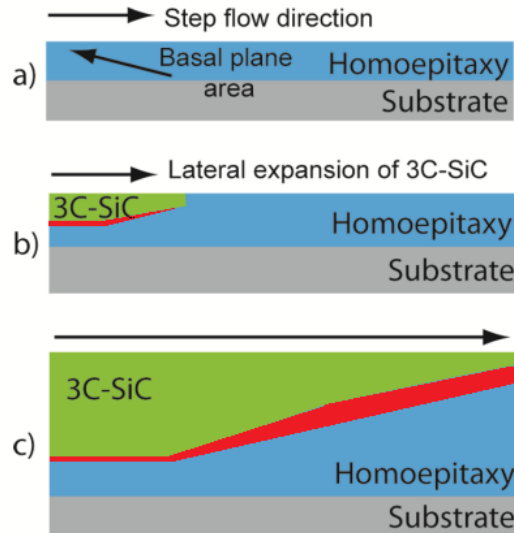


Figure 8: A model for the growth of cubic SiC on hexagonal substrates in three steps: (a) Building of a basal plane, (b) Nucleation of 3C-SiC and (c) growth of 3C-SiC in step-flow direction [57].

Figure 8 describes the growth on an off-axis hexagonal SiC substrate. The growth starts by a formation of a large terrace with a basal plane at the left edge of the substrate, with the step-flow direction to the right side (Fig. 8a). This terrace forms because of an interaction between the spacer and the substrate. The substrate itself features small steps from the beginning which grow during the temperature ramp up. The graphite spacer (Chapter 2.1) prevents the step-flow growth of 4H-SiC on the left edge of the substrate, leading to a large terrace. This large terrace is needed to nucleate cubic SiC with 2D island nucleation growth, as there is a high supersaturation needed to form it on the rather small standard steps of e.g. 4° off-axis 4H-SiC substrates (Fig. 8b) [44]. After the formation of one or more nucleation sites on the left side of the substrate the cubic SiC grows in step-flow direction and covers the whole substrate depending on the growth time and the growth rate (Fig. 8c). Between the homoepitaxial grown material and the heteroepitaxial grown 3C-SiC a transition layer can be found (red part in figure 8). This transition layer is a typical boundary to overcome the rather small but existing lattice mismatch.

The lateral coverage (X) of the substrate can be calculated by equation 6 [9], using the thickness H , where the basal plane is formed with an off-axis angle α .

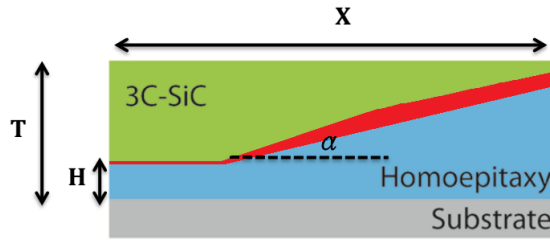


Figure 9: Cross-sectional view of as-grown 3C-SiC with the lateral coverage X , the layer thickness T , the thickness of the homoepitaxial layer H , the off-axis angle α and the transition layer (red area)[9].

It has been determined that the homoepitaxial growth on 4° off-axis 4H-SiC substrates is around $60\mu\text{m}$ [9]. By using equation 6 a total thickness T of around 1mm has to be achieved (Fig. 9) to cover the whole substrate (10x10mm).

$$X = \frac{T - H}{\tan(\alpha)} \quad (6)$$

For a good quality of the as-grown 3C-SiC the desirable amount of nucleation sites on the basal-plane should be close to one and the quality of the substrate should be very good. Therefore they should not feature any defects or contaminations.

INFLUENCE OF SUBSTRATE-MATERIAL

For the homoepitaxial growth of 3C-SiC, substrates of a very high quality are needed. Crystals of 4H- and 6H-SiC with a dislocation density below 10^2cm^{-2} area are available [37, 47]. Moreover, SiC substrates like 4H-, or 6H-SiC are very well suited for the growth of 3C-SiC, due to a low memory effect [45]. Compared to the use of pure silicon substrates, SiC also features a very small lattice and thermal mismatch making it ideal for an epitaxial growth.

A study of 3C-SiC growth using on-axis 4H-, and 6H-SiC substrates presented by R. Yakimova et al. supports the idea of a favored growth of 3C-SiC in silicon rich environment, which had also been stated by A. Fissel before [45, 19]. It was also determined that cubic substrates favor the formation of stacking faults, resulting in a mixture of polytypes, e.g. 6H-SiC inclusions [45]. This leads to the use of 4H- and 6H-SiC substrates,

growing on the Si-face in a supersaturated ambient, to favor the formation of the cubic polytype. As a result of the growth mechanism of 3C-SiC the use of on-axis substrates most likely leads to the inclusion of other polytypes (4H- or 6H-SiC), as well as the formation of many nucleation sites and therefore high density of grain boundaries in the as-grown 3C-SiC [45].

However, the as-grown 3C-SiC needs to feature single crystalline properties to be of further use in applications. Hence, off-axis substrates with the already discussed growth mechanics are used (Chapter 2.2) to lower the amount of nucleation sites and favor the step-growth. The theoretical approach to produce single crystalline 3C-SiC would be to form exactly one nucleation site and then continue the growth, but the formation of only one growth site is difficult to achieve and needs further investigations.

The main difference between 4H-SiC and 6H-SiC substrates is the stacking of the silicon and the carbon bi-layers in the material. Figure 10 shows three different stacking possibilities labeled as 3C, 4H and 6H [17, 47]. Here, 3C-SiC has the stacking sequence of ABC (C_3), whereas 4H-SiC has ABCB (C_4) and 6H-SiC has ABCACB (C_6). However, the 6H-SiC stacking sequence is built by the two possible ways to stack 3C-SiC (ABC and ACB) [47]. This leads to the assumption that the growth of cubic SiC should be favored on those substrates.

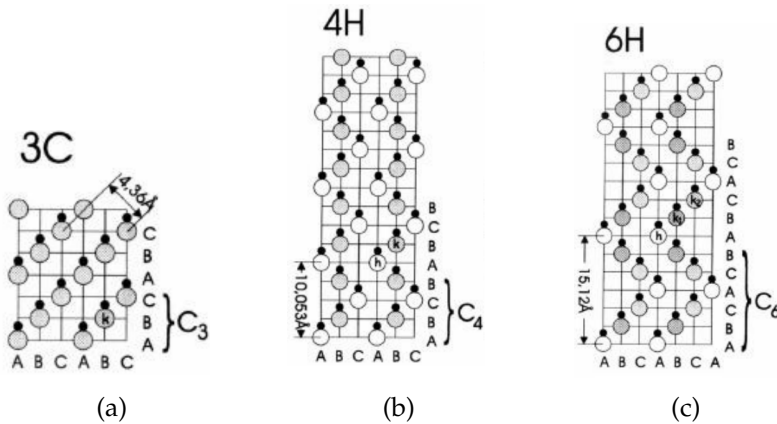


Figure 10: Two hexagonal (4H and 6H) and one cubic (3C) polytype of SiC and their different stacking sequences using the typical, triangular unit cell [37].

Furthermore, the on-axis surface energy (Ω) of 6H-SiC is lower than the one of 4H-SiC ($\Omega_{\text{6H}} = 1767 \frac{\text{erg}}{\text{cm}^2}$; $\Omega_{\text{4H}} = 1800 \frac{\text{erg}}{\text{cm}^2}$), resulting in a lower critical level for the supersaturation α_{crit} mentioned in equation 4 [46].

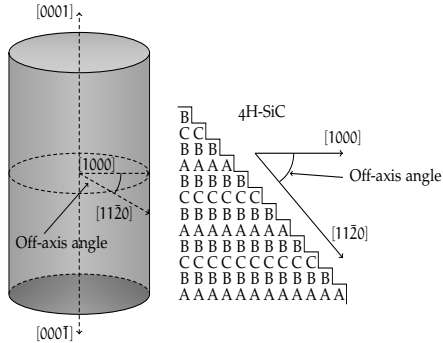


Figure 11: Schematic illustration of a 4H-SiC crystal ingot with the growth direction [0001], the on-axis direction [1000] and the off-axis direction [11\bar{2}0].

Figure 11 shows the geometric properties of the off-axis cut out of a 4H-SiC ingot, leading to a $[11\bar{2}0]$ surface on the substrates. Those substrates show the characteristic steps which are also illustrated in figure 11.

3

DOPING OF 3C-SiC IN SUBLIMATION EPITAXY

There are two different ways to introduce dopants using sublimation epitaxy. The first and the most common approach is to use a doped source material (e.g. boron doped polycrystalline SiC) [51, 39]. The second way is to introduce gases (e.g. nitrogen) into the growth chamber, which can penetrate the porous carbon crucible.

The level of the doping during the growth process depends on the partial vapor pressure of the dopant species, on the temperature and on the $\frac{Si}{C}$ ratio [64]. The latter is caused by the site competition effect between Si, C and the dopants, leading to an inhomogeneous doping of SiC. Therefore, a growth on the Si-face does not favor the incorporation of nitrogen on C-sites, whereas aluminium and boron choose the Si-sites [51, 13, 27, 33]. This effect is used in the site-competition epitaxy model, using the $\frac{Si}{C}$ ratio to control and regulate the concentration of the dopant incorporation into the lattice sites. This implies an outcompeting of nitrogen by carbon, due to an increase of the carbon concentration and an outcompeting of boron by silicon, due to an increase of the silicon concentration [13]. This model also supports the work of Choyke and Davis using spectroscopic measurements to find out that nitrogen occupies C-site [11, 16].

In order to obtain uniform doping an homogeneous temperature field has to be applied. However, according to the numerical simulations the introduction of different source-material morphologies (e.g. solid polycrystalline or powder) have a big influence on the temperature field due to transitions during the growth [49, 40]. Therefore, the temperature field in the growth chamber depends on the density of the used, doped or undoped source material. By means of the introduction of a boron doped microcrystalline ($\leq 100\mu m$), SiC powder can lead to a lower quality of the epitaxial layer than the introduction of a solid, doped or undoped macrocrystalline SiC source [40, 56].

Recent research compared three different source materials to grow fluorescent SiC (f-SiC) for the use in white light emitting diode (LED) production: (i) High temperature hot pressing (HTHP), (ii) chemical vapor deposition (CVD), and (iii) physical vapor transport (PVT) [56]. For the first source material a problem occurred, regarding the carbon rich binder material, used to agglomerate the SiC and the boron powder during the pressing process. This binder cracks during the growth and changes the $\frac{\text{Si}}{\text{C}}$ ratio and can also lead to a termination of the growth itself, due to graphitization of the source [56]. The advantage of the CVD and the PVT grown sources is the absence of binding materials and a higher stoichiometric match between the source and the as-grown f-SiC. Consequently an uniform sublimation rate and a uniform impurity incorporation can be achieved more easily. Moreover, higher growth rates of approximately $200 \frac{\mu\text{m}}{\text{h}}$ can also be achieved [56].

The difference between a CVD and a PVT grown source is determined by the average size of the crystal domains. While a CVD grown source material shows grain sizes from $1\mu\text{m}$ to $10\mu\text{m}$, the material grown by PVT features grain sizes ranging from $500\mu\text{m}$ to 4mm [56]. In respect of those numbers PVT grown source materials can lead to a higher uniformity in doped growth of SiC. In polycrystalline nitrogen and boron co-doped SiC source, grown using the PVT growth method, it was observed that the growth rate depends on the inclination direction of the subliming grains [32].

4

DEFECTS IN SiC

During the growth of SiC different types of defects can occur leading to additional energy levels in the bandgap. The most efficient bandgap configuration was already discussed in chapter 1. Therefore, a deep energy level at one third above the valence band is preferred. Hence, the appearance of defect levels will lower the performance of later produced IBSC material. Especially defect complexes due to high dopant incorporation need to be accounted. The defects in SiC can be subdivided into two groups: (i) The structural defects (grainboundaries, stacking faults,...) and (ii) the interstitial defects produced by introducing dopants into the lattice sites (e.g. nitrogen or boron).

The initial growth process of β -SiC leads to many nucleation sites on the basal plane. During the 2D-Island growth different crystal islands will coalesce or form twin boundaries in between [59, 9, 10]. If a twin boundary, or a so called double positioning boundary (DPB) forms, the crystal orientation is shifted by 60° and will continue to spread over the crystal [47]. Eventually it will cover the whole substrate surface (depending on the growth time), featuring different crystal domains and grain boundaries. Cubic SiC can only form twinned domains because of the two possibilities to arrange the SiC bilayers: Either (i) ABCABC or (ii) ACBACB [59].

While the stacking sequence of β -SiC is either ABCABC or ACBACB, the array for $4H$ -SiC is ABCBA and ABCACB for $6H$ -SiC, which was already mentioned in chapter 2. If the stacking sequence along the c-axis is interrupted, a so called stacking fault (SF) is formed. These kinds of defects are quite common in SiC because they feature low energies. Typical energies for the three different SFs for $6H$ -SiC are therefore $40 \frac{mJ}{m^2}$ and $3 \frac{mJ}{m^2}$, for $4H$ -SiC the two SFs have energies of around $18 \frac{mJ}{m^2}$ and the one SF for β -SiC has the energy of $-1,7 \frac{mJ}{m^2}$ [59, 41, 23]. So the cubic system releases energy to form a stacking fault. Those defects can influence the bandgap and lead to a parasitic recombination. Moreover, they can act as scattering centers for

charge carriers and lower their mobility [59, 38].

Another type of defect, which can occur during the growth of β C-SiC is an inclusion of other polytypes. This happens if the growth conditions change ($\frac{\text{Si}}{\text{C}}$ -ratio, temperature, supersaturation, ...) and the polytype growth of the substrate is favored. If the conditions are appropriate the substrate polytype will be overgrown and be included into the transition layer instead [59, 23].

For a functional IBSC a boron concentration of at least $10^{20} \frac{1}{\text{cm}^3}$ is needed. Such a high dopant concentration leads to a high disturbance of the crystal structure and therefore to many defects like vacancies (V), interstitial addatoms (I) or defect complexes. Recent research in the growth of hexagonal SiC (4H-SiC and 6H-SiC) showed that boron doping leads to a deep donor level (D-center) in addition to a shallow boron acceptor level [51, 5]. The latter is assigned to a silicon lattice site (B_{Si}), whereas the D-center could theoretically consist of a boron atom combined with intrinsic defect (e.g. V_C) forming a defect complex [28, 50]. The doping process of β C-SiC however features a lack of knowledge.

Part III

EXPERIMENTAL

5

HETEROEPITAXIAL GROWTH OF 3C-SiC

Cubic Silicon carbide was grown using sublimation epitaxy at different temperatures. The substrate material was produced by a German company called SiCrystal. It is a high quality 4H-SiC with an off-axis angle of 4°. Some of the material properties are listed in table 1.

Table 1: Substrate Properties for the 4H-SiC material used as seeding material for the growth of 3C-SiC produced by the company SiCrystal [4].

Properties	Substrate
Polytype	4H
Diameter	100 ± 0,5mm
Thickness	700 ± 50µm
Carrier Type	n-type
Dopant	Nitrogen
Wafer Orientation	4 ± 0,5 °
Micropipe Density	≤ 1cm ²
Micropipe Free Area	≥ 95%
Surface	Si-face CMP Epi-ready, C-face matted

The substrates were cut into $10 \times 10\text{mm}^2$ samples from the same wafer and cleaned with acetone and ethanol followed by $\text{H}_2\text{O} : \text{NH}_3 : \text{H}_2\text{O}_2$ (5:1:1), $\text{H}_2\text{O} : \text{HCl} : \text{H}_2\text{O}_2$ (6:1:1). For the growth the Si-face of the substrate was used to favor the formation of 3C-SiC.

The source material was produced by Mitsui and is stated as ultra high purity non porous SiC. The production technique is a CVD method and it provides material with a thickness of $700 \pm 50\mu\text{m}$. The impurity content is listed in table 2.

In the first step of the growth of the 3C-SiC, a preparation of the approximately 500µm thick tantalum foil is needed, to prevent it from bending during the actual growth process and therefore, to provide a homogeneous sublimation on the substrate. For

Table 2: Impurity content in Mitsui source material [24].

Na	Co	K	Cu	Zn	Mn	Fe	Cr
< 2ppb	1,3ppb	< 60ppb	< 50ppb	9ppb	< 9ppb	35ppb	6ppb

this pretreatment a circular piece was cut out from the foil and placed in the crucible. The top surface of the foil was covered with pieces of source material. Furthermore, the spacer and a graphite plate were placed on top. The crucible was closed up and introduced into the vacuum chamber until the pressure in the growth chamber reached a value of 10^{-5} mbar. A fast temperature ramp up was applied and the temperature was maintained for 10 minutes at 2000°C . An exchange of the tantalum foil was made after an actual growth run longer than four hours to provide a high silicon saturation in the gas species.

The next step was the actual growth of the 3C-SiC with a thickness of approximately 1 mm. Two sources with a total thickness of $1400\mu\text{m}$ ($\pm 100\mu\text{m}$) were stacked and introduced above the pretreated and therefore partially to tantalum carbide converted tantalum foil. The spacer was placed on top of the sources containing an opening of $7 \times 7\text{mm}^2$ or $5 \times 5\text{mm}^2$. This opening was closed with the 4H-SiC substrate with the Si-face down. A graphite plate was placed on top of the substrates to prevent a backside sublimation during the growth. After the filling of the crucible, it was inserted into an insulation foam and the quartz tube.

Figure 12 shows a graph of the growth temperature over the growth time for the major part of the experiments. The temperature was measured on top of the crucible using a pyrometer. The ramp up and the adjustments were made by a manual RF generator. During the growth runs a vacuum of 10^{-4} mbar to 10^{-5} mbar was maintained using a turbo pump. For the growth runs a temperature ramp up of $20\frac{{}^{\circ}\text{C}}{\text{min}}$ was used until the designated growth temperature of around 1700°C to 2000°C was reached. Then the temperature was kept with a tolerance of $\pm 3^{\circ}\text{C}$. For the cool down the RF generator was turned off and a waiting time of approximately two hours was stated.

After the growth run a re-sublimation process can be used to remove possible deposited layers on the spacer and the graphite plate. Therefore, the contaminated parts of the setup get intro-

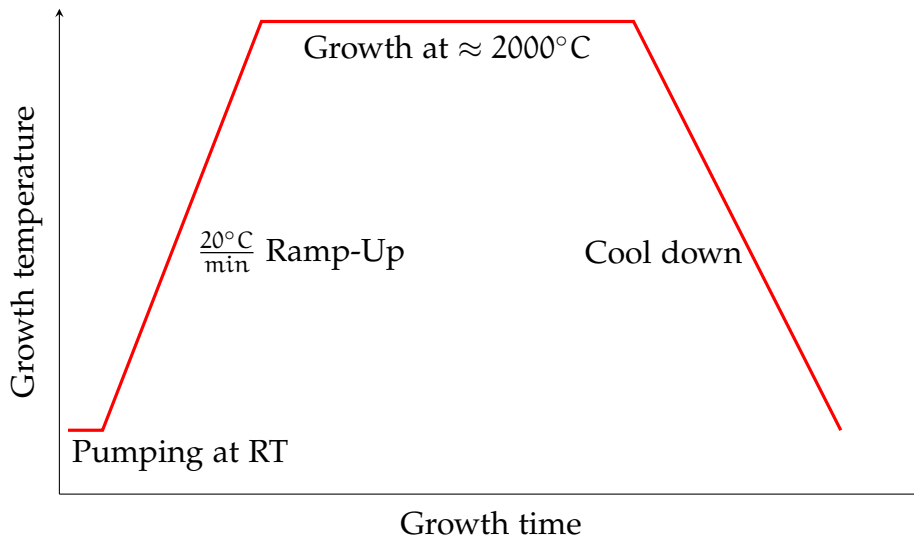


Figure 12: Growth temperature over growth time during the actual growth of 3C-SiC, starting with the pumping at room temperature, followed by the ramp up until the growth temperature is reached. In the end a cool down is made for approximately two hours.

duced into a dummy crucible with the deposited layer facing to the top and are heated up to approximately 2000°C . This temperature is held for 15 to 25 minutes, depending on the degree of deposition and cooled down afterwards. The deposited layer will re-sublime and crystallise on the top of the crucible.

Table 3: Summary of the experiments and sample IDs, which were made during the growth of 3C-SiC seeding material to characterize and estimate the properties and possible defects in the crystal.

Sample ID	Process-Setup	Theme
ELS525-ELS532	Old Reactor	Estimation of growth rate
ELS533-ELS545	New Reactor	Estimation of growth rate
ELS537-ELS545	New Reactor	Estimation of Crystall Quality
ELS537,ELS539,ELS542	New Reactor	KOH Etching for SFs
ELS546	New Reactor	Optimization of the growth time
ELS547-ELS548	New Reactor	Growth of Epi-Layer

In the first experiments the actual growth rate for the setup was estimated using three different temperatures: (i) 1850°C , (ii) 1900°C and (iii) 1950°C . The temperature ramp up and pressure was kept the same. Therefore, a good comparison is possible. The

thickness of the samples was measured using a micrometer and calculating the mean value of four measurement points.

Later on, the morphology of the 3C-SiC was characterized using optical microscopy. Analysis of the optical micrographs was used to make comparisons of DPBs in different samples.

At the end the stacking faults of those as-grown samples were made visible by etching them for 1 minute in KOH at 500°C. The analysis of those samples was made by optical measurements and an analysis software called Igor Pro, which transformed the pictures into grey scaled copies and counted the closed up particles.

6

HOMOEPITAXIAL GROWTH OF BORON DOPED β C-SiC

For the growth of homoepitaxial boron doped β C-SiC layers, the as-grown β C-SiC material (discussed in the chapter before) was used as a seeding material. The thickness of the seeding β C-SiC was approximately $800\mu\text{m} - 1000\mu\text{m}$. Therefore, to provide enough space for the growth of boron doped layer, a 2mm spacer was used. The boron-doped source material was produced by the university of Erlangen as shown in figure 13 (c).

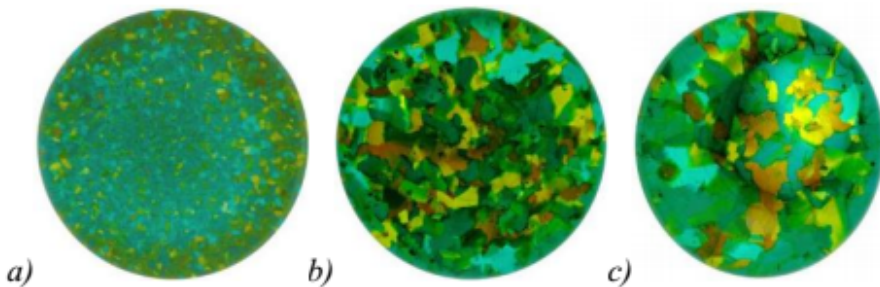


Figure 13: High resolution pictures of the source material at different stages during the enlargement process in the growth process. (a) After nucleation, (b) after approximately 10 hours and (c) after approximately 20 hours of growth with a composition of 4H, 6H and 15R [32].

The source material is grown using the modified physical vapor transport and features a microcrystalline property with the main composition of 4H-, 6H- and 15R-SiC. Figure 13 shows the three different steps during the growth of this source material. Therefore, the initial step of this process is the nucleation, (fig. 13 (a)) which is followed by an additional growth to enlarge the grains (fig. 13 (b) and (c)). The boron concentration in the material is approximately $3 \cdot 10^{18} \frac{1}{\text{cm}^3}$.

For the homoepitaxial β C-SiC growth process a temperature ramp up of $\frac{20\text{K}}{\text{min}}$ and a growth temperature of 1850°C was used. To distinguish the influence of the pressure on the mean free path of the gas species during the growth, different pressure adjustments were set denoted as followed: (i) Dynamic pressure,

(ii) static pressure, (iii) pressure 1000, (iv) pressure 1200 and (v) nitrogen atmosphere. Dynamic pressure describes, the growth chamber in a constant pressure of 5×10^{-5} mbar, whereas static pressure depicts a closing of the pumping valve before the temperature ramp up. For the procedure of pressure 1000 and pressure 1200 the valve of the pump was closed at approximately 1000°C and 1200°C. The growth in nitrogen ambient was started at an initial pressure of 5×10^{-3} mbar.

Table 4: Summary of the experiments and sample IDs of the executed experiments to research the incorporation of doping species into the crystall lattice by varying the pressure during the growth.

Sample ID	Process-Setup	Growth time
ELS541, ELS536	Dynamic pressure	1 hour
ELS547	Static pressure	1 hour
ELS545	Pressure 1000	1 hour 30 minutes
ELS546	Pressure 1200	1 hour 30 minutes
ELS529	Nitrogen ambient	1 hour 30 minutes

Due to the influence of the growth rate by the pressure the growth times had to be adjusted to provide a thickness of approximately 200µm to 300µm. This way, a decent characterisation of the as-grown doped layers by photoluminescence (PL) measurements is possible.

Part IV

RESULTS AND DISCUSSION

7

GROWTH CONDITIONS FOR THE β C-SiC SEEDS

The starting point of the experiments in this thesis was aimed for determination of the growth rate and the optimal growth temperature for β C-SiC. For the first purpose, three various temperatures were used (1850°C , 1900°C and 1950°C) and crystals were grown using different growth times in order to obtain similar thicknesses. Afterwards the sample thickness was measured at different points. The average value of the thickness is presented in table 5. The first series, however, were grown in an unstable reactor, leading to significant variations in growth rates at the same temperature (table 5).

Table 5: Summary of the first sample series grown in an unstable reactor.

Sample ID	ELS525	ELS526	ELS527	ELS528
Temperature	1950°C	1950°C	1900°C	1850°C
Time	110min	80min	60min	60min
Thickness	$1550\mu\text{m}$	$1500\mu\text{m}$	$1100\mu\text{m}$	$650\mu\text{m}$
Growth rate	$\geq 845\frac{\mu\text{m}}{\text{h}}$	$\geq 1125\frac{\mu\text{m}}{\text{h}}$	$\geq 1100\frac{\mu\text{m}}{\text{h}}$	$\approx 650\frac{\mu\text{m}}{\text{h}}$
Power input	$\approx 1200\text{W}$	$\approx 1200\text{W}$	$\approx 1200\text{W}$	$\approx 1000\text{W}$
Sample ID	ELS529	ELS530	ELS531	ELS532
Temperature	1850°C	1950°C	1950°C	1950°C
Time	95min	25min	20min	20min
Thickness	$1000\mu\text{m}$	$1400\mu\text{m}$	—	—
Growth rate	$\approx 631\frac{\mu\text{m}}{\text{h}}$	$\approx 3360\frac{\mu\text{m}}{\text{h}}$	—	—
Power input	$\approx 1000\text{W}$	$\approx 1300\text{W}$	$\approx 1400\text{W}$	$\approx 1700\text{W}$

Due to high growth rates, some of the β C-layers (with thickness over 1mm) overgrew the spacer which leads to formation of various defects on the layer surface (fig. 14 b). The samples with a thickness equal or below to 1mm show a good quality compared to the overgrown or graphitized ones, like ELS529 (fig 14 a). The black dots on the image in figure 14 a, are formed on the backside of the sample. This backside sublimation also

increases with higher power input due to a changed temperature field in the crucible. Also, the actual growth rate increases significantly while going up with the growth temperature from 1850°C to 1950°C. In the end the power input needed to maintain the same temperature went up to a value of 1700W, leading to a high graphitization of the source and the sample. Therefore the generator was exchanged due to its unreliability during the growth process.

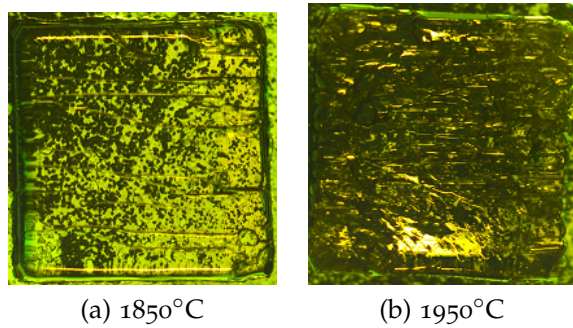


Figure 14: Samples of the size $7 \times 7\text{mm}^2$ grown at (a) 1850°C showing a good quality with a small amount of backside sublimation of the substrate material and (b) 1950°C, featuring a bowl like surface due to the overgrowth of the spacer (higher growth rate) and a higher amount of backside sublimation.

After an exchange it was possible to grow at stable conditions and stable growth rate ($\pm 200\mu\text{m}$). The growth rates for (i) 1850°C, (ii) 1900°C, and (iii) 1950°C are plotted in fig. 15.

The fluctuation of $\pm 200\mu\text{m}$ for the growth runs at higher temperature can be explained by the exhaustion of the tantalum foil during long growth runs and the change of $\frac{\text{Si}}{\text{C}}$ ratio. The longer the use of the foil, the less pure tantalum is left which can gather carbon atoms. It was found that 3C-SiC favors to form at a silicon rich gas species [44]. However, there is no mathematical approach to this phenomenon yet. The exhaustion of tantalum leads to a decrease in $\frac{\text{Si}}{\text{C}}$ ratio in the gas phase. This lowers the probability to form 3C-SiC. Also, the foil was not exchanged after each run, leading to a small amount of variation during these growth runs.

In figure 15 the growth rate follows the rule of thumb presented by M. Syväjärvi for 4H- and 6H-SiC [35]: The growth rate dou-

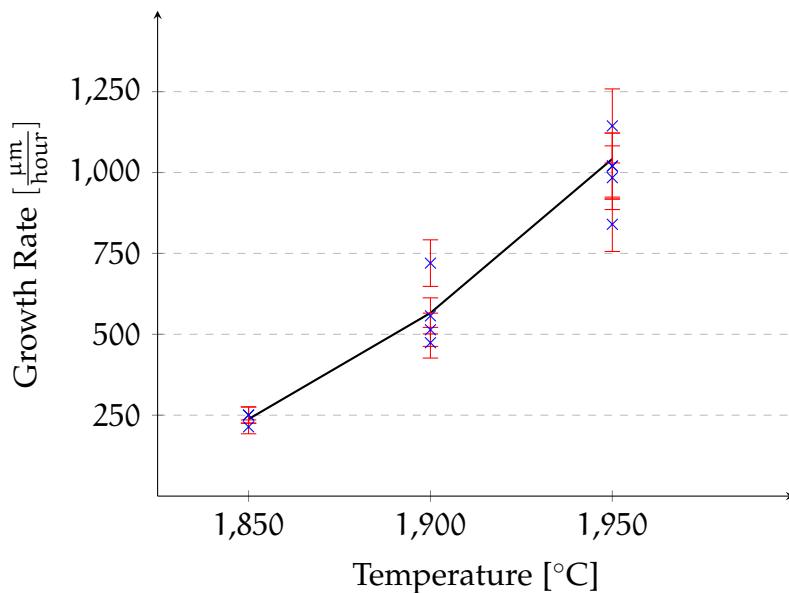


Figure 15: Growth rate over temperature for the samples series ELS533-ELS545 using the new generator. The increase in growth rate follows results presented in [35].

bles by an increase of the temperature by 50°C. Therefore, a realistic dependency is an exponential progression of the growth rate, due to the exponential dependencies to the temperature and the supersaturation of the growth (fig. 7 and equation 4).

The surface coverage with 3C-SiC is proportional to the thickness of the as-grown layer. Figure 16 shows a cross-sectional cut of a grown sample. The growth temperature was 1950°C at a growth rate of approximately 1000 $\frac{\mu\text{m}}{\text{hour}}$.



Figure 16: Crosssectional view on a 600 μm thick sample grown at 1950°C, showing the homoepitaxial growth on the 4H-SiC substrate followed by the transition layer, which gets covered by the heteroepitaxial growth of 3C-SiC.

The as-grown crystal is 600 μm thick and features a small amount of cubic silicon carbide (yellow part). Beneath the yellow part there is a transition layer which is grown on the homoepitaxial 4H-SiC. The aim of the executed experiments was to grow a sample with a surface which is fully covered with 3C-SiC. For

this at least a 1mm thick layer is needed.

An indication for the lateral overgrowth of the surface is the visibility of the transition lines at the end of the sample in step-flow direction. Figure 17 shows the defect rich area at the right side of the samples (fig. 16).

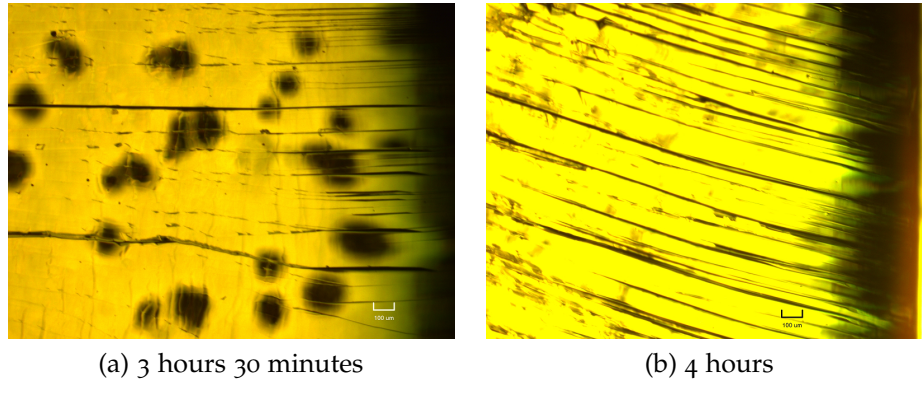


Figure 17: 50× magnification of samples grown at 1850°C for (a) 3 hours and 30 minutes and (b) 4 hours, showing defects in the transition layers.

The black dots in figure 17 (a) are defects revealed by the back-side sublimation of the substrate during the growth. The lines which are parallel to the growth direction are located in the transition layer. This region features many defects and therefore needs to be overgrown by the 3C-SiC. A thickness of around 1 mm as-grown crystal was estimated to be thick enough to show such characteristics, using equation 6.

In the end the growth time at 1850°C was 4 hours, for 1 hour 50 minutes at 1900°C and 50 minutes at 1950°C. The pressure for the homoepitaxial growth was kept dynamic, which means that the turbo pump was evacuating the growth chamber at all times. Furthermore, no gas was introduced. However, there is a background contamination in the reactor which usually leads to residual doping concentrations up to $10^{16} \frac{1}{\text{cm}^3}$.

8

MORPHOLOGY AND DEFECTS IN β C-SiC SEEDS

INFLUENCE OF TEMPERATURE ON THE FORMATION OF DPBS

The quality of β C-SiC layers can be initially evaluated by estimating the density of double-positioning boundaries (DPBs). Optical microscopy with Nomarski Interference Contrast ($\times 50$, $\times 200$, $\times 500$ and $\times 1000$ magnification) was used to take a first look at the surface. In this way the polytype inclusion and the formation of grain boundaries was analyzed. For a more proper way of characterisation Photoluminescence measurements at room temperature (RT), 77K and at 23K were made and compared to 2K measurements of previous experiments.

The density of DPBs changes by growing β C-SiC at different temperatures (fig. 18).

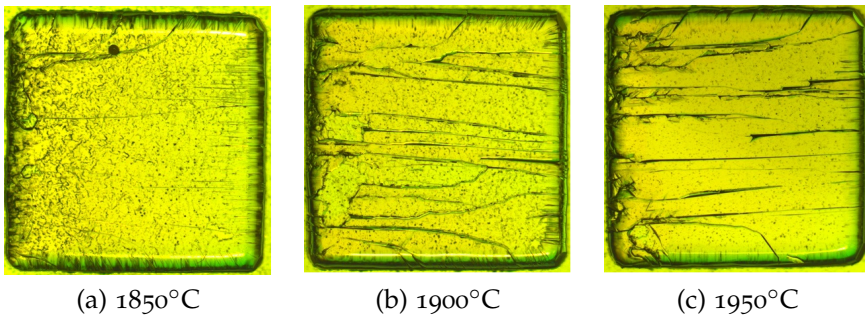


Figure 18: Pictures of β C-SiC grown at three different temperatures (1850°C , 1900°C and 1950°C) obtained optical microscopy showing different amount of DPBs on a sample size of $7 \times 7\text{mm}^2$.

The lowest amount of DPBs was found in β C-SiC crystals grown at the lowest temperature (1850°C) and the highest amount was found at the highest growth temperature (1950°C). This means, that the DPBs formation correlates with the growth temperature and growth rate. Figure 19 shows the Number of domains over the temperature.

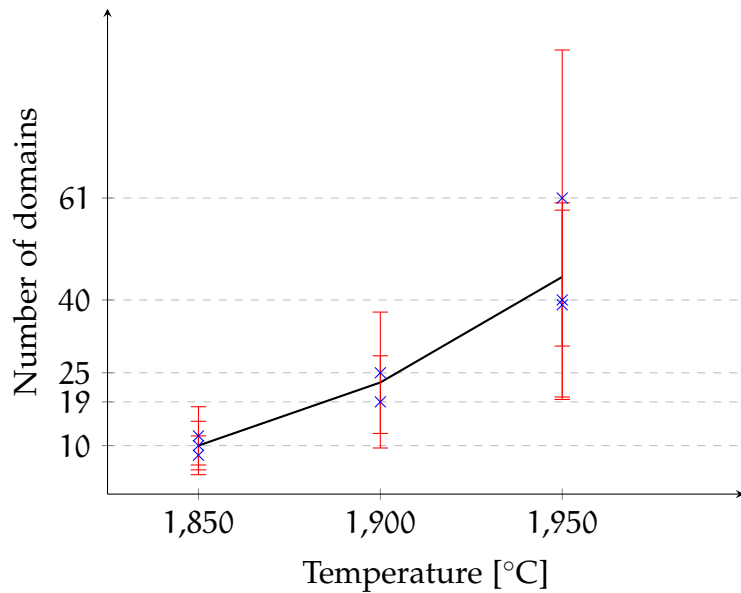


Figure 19: Number of domains from samples grown at three different temperatures.

An exponential increase of the domain boundaries by increasing temperature is visible. Therefore, the lowest temperature used in the experiments shows the smallest amount of DPBs.

In the general aspects part of this thesis the equation for the critical supersaturation was stated (equation 4). By increasing the temperature from 1850°C over 1900°C up to 1950°C, the critical value for the supersaturation decreases, leading to a silicon richer gas species. It is well known that, the higher the silicon concentration in the gas phase, the higher the probability to form cubic silicon carbide. Therefore with a lower critical supersaturation value, more nucleation sites are formed on the substrate surface. The incoming gas molecules arrive at the surface and diffuses along it. With a higher amount of nucleation sites, more islands can form and grow. The density of grains increases.

EVALUATION AND DEVELOPMENT OF SFS

For the evaluation of the stacking faults, three samples grown at 1850°C, 1900°C and 1950°C were etched in Kaliumhydroxide (KOH) at approximately 500°C for 1 minute. The etching rate for this experiment is estimated to be around $1.15 \frac{\mu\text{m}}{\text{min}}$ for a not

defected crystal [14]. This process allows to make defects like stacking faults visible [15].



Figure 20: Optical micrograph ($\times 50$) of KOH etched sample grown at 1850°C for 3 hours and 30 minutes, showing stacking faults and their increase over the sample length in step-flow direction.

Figure 20 shows the sample grown at 1850°C in a $\times 50$ magnification. Each triangular formation on the surface determines a stacking fault and therefore, an interruption of the stacking sequence for 3C-SiC. The optical microscope pictures for the other two samples look similar and are therefore not shown. The reason for the characteristic formation of this etched surface is the fact that a stacking fault is also a defect in the bulk crystal. Therefore, it lowers the binding energy to the bulk and leads to a higher etching rate for this area. The stacking faults are governed by partial dislocations from dissociated basal plane dislocations. In the (111) basal plane the partial dislocation lines form 60° angles. Therefore the triangular shapes of the SFs.

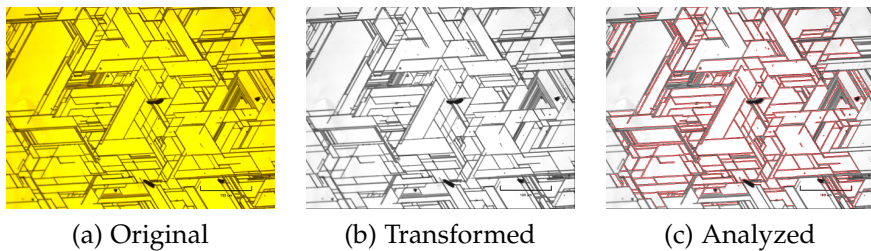


Figure 21: (a) $200\times$ magnification of stacking faults, made visible using KOH. (b) Transformed into grey scale. (c) Analyzed by using the software Igor Pro.

Figure 21 (a) shows a $\times 200$ magnified picture of the surface after the etching process. Clearly visible are the triangular shaped defects, which correspond to stacking faults in the material. The smallest building unit in SiC is a three-sided pyramid with a silicon atom in the center and four carbon atoms forming the edges. Out of this unit the different polytypes of silicon carbide are formed by a tetrahedral stacking sequence. 3C-SiC features

the zinc-blende structure with the formation of ABCABC or ACBACB. In this polytype there is only one possibility to produce a stacking fault by partial dislocation glide [55] (fig. 22).

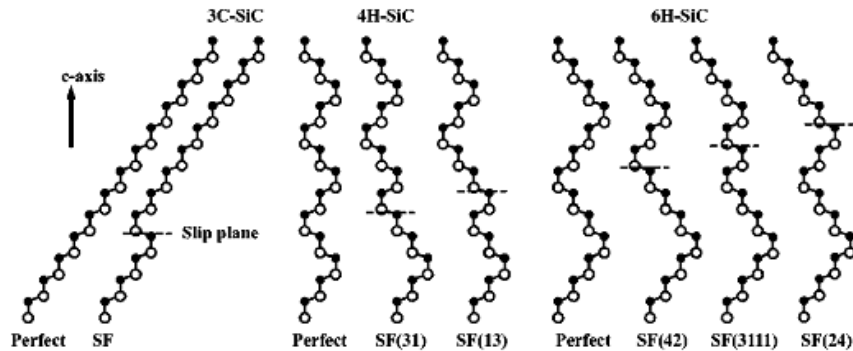


Figure 22: Schematic view of the three main polytypes and their corresponding stacking faults (dashed horizontal lines) viewed from a $[11\bar{2}0]$ direction [55]

Therefore, by etching the as-grown samples featuring a $\{111\}$ surface the introduced stacking faults (SFs) show a higher etching rate compared to the perfect stacking sequence of the cubic part, showing triangular shapes, due to the geometries of the unit cell, the stacking of the polytype and the surface orientation [42].

For the evaluation of the stacking fault density over the samples a software called Igor Pro was used. Figure 21 shows the procedure of modifying the taken pictures of the sample surface and the way of analysis. Picture (a) is a $\times 200$ magnified optical picture of the surface featuring a high density of SFs. In the next step (fig. 21 (b)) the picture was transformed into a grey-scaled figure to enable the postprocessing. In the last process step the average size of the counted objects have to be adjusted. For the purpose of our experiments a minimum dot size of 20pixels was used. In this way inclusions or dust particles are taken out of the counting process. Afterwards the programm counted all rectangular objects in the sample without the border areas and summed them up (fig. 21 (c)). However, this number is not the exact amount of grain boundaries, because it also counted enclosed areas which result from overlapping of different SFs, but the trend from sample to sample can be indicated.

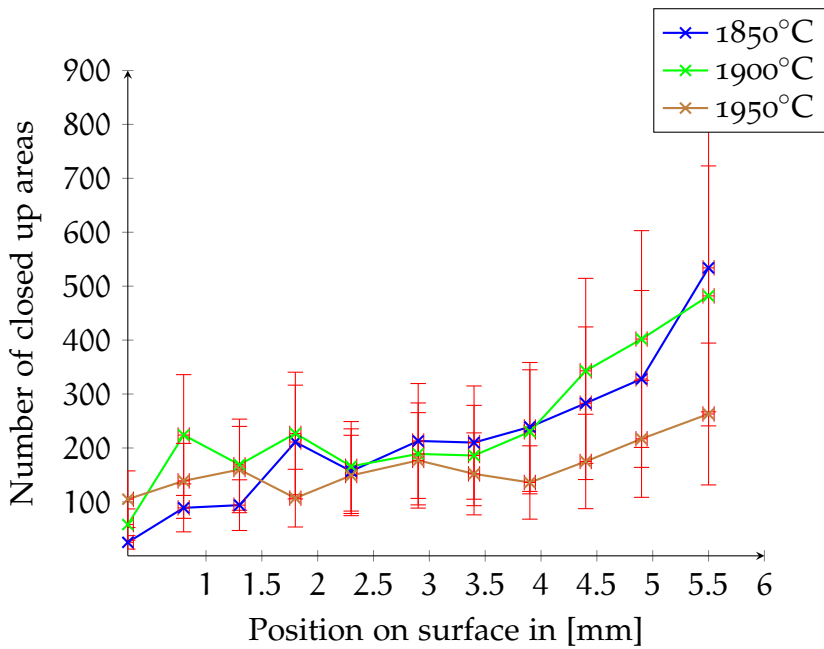


Figure 23: Number of closed up areas on the surface of three samples grown at different temperatures and etched with KOH for 1 minute.

Figure 23 shows the amount of enclosed areas over the surface area from the nucleation side in the step-flow direction and therefore, the growth direction. A clear increase in the amount of closed up areas is visible, means an increase of SFs. There is also no clear dependency between the amount of SFs and the growth temperature. However, a clear dependency in the amount of SFs and the thickness is visible (fig. 23 and fig. 16). This effect was already observed for 3C-SiC grown on silicon substrates using CVD describing the formation of SFs in hetero-interface as a consequence of the misfit and a decrease of SF density with increasing thickness [3]. A saturation of the density in the range of $10^3 \frac{1}{\text{cm}^2}$ to $10^4 \frac{1}{\text{cm}^2}$ was also observed.

For a better estimation of the SFs on 3C-SiC with this orientation a picture evaluation software is needed which is able to count the amount of triangulairs with a fixed angle. This way a density of SFs and a better characerization of the as-grown material would be possible. Another aspect for engineering the SF density would be the influence of the substrate and the characteristic misfit.

PL-, RAMAN AND CL-MEASUREMENTS OF THE SEEDING MATERIAL

For a proper capture of the as-grown crystal quality, PL measurements at different temperatures and positions on the sample were made. The measurement equipment uses a 405nm laser combined with a short pass filter for the range of 400nm to 450nm and a long pass filter for the range of 450nm to 2000nm. Moreover a spot size of approximately 50 μ m and a dectector with a range up to 800nm was used. Combined with a closed-cycle cryostat, temperatures down to 23K could be achieved.

Figure 24 shows the first measurement of samples grown at 1850°C, 1900°C and 1950°C. The measurement was produced at room temperature and shows a broad peak in the region from 450nm to 550nm with a maximum at approximately 500nm.

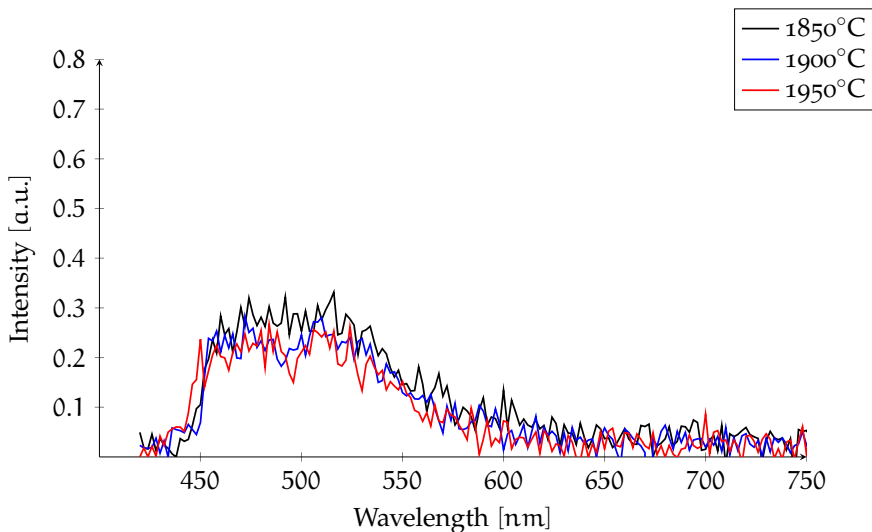


Figure 24: Intensity over wavelength for a photoluminescence measurement at room temperature ($T=300\text{K}$) of three samples grown at different temperatures, showing a broad peak in the blue wavelength area due to DAP of 4H- or 6H-SiC.

The indirect bandgap of silicon carbide leads to a low probability of radiative recombination after excitation by a laser at room temperature. Therefore, the peaks in figure 24 are most

likely characteristic for the donor acceptor pair photoluminescence (DAP) or impurities of different polytypes like 4H-, or 6H-SiC on the sample and from the 4H-SiC substrate.

To distinguish the existence of other polytypes, Raman measurements were done on the sample grown at 1850°C (fig. 25). For the measurement a helium neon laser with a wavelength of 633nm was used.

The Raman modes, shown in figure 25, were measured at the end of the sample (in growth direction) showing all polytypes which were found on this sample. The peaks are characteristic for 3C-, 4H- and 6H-SiC. The first peak could also resemble 2H-SiC. The 4H-SiC peak can be reasoned by the used substrate and the subsequent transition layer, whereas the 6H-SiC peak could be a response to the SFs.

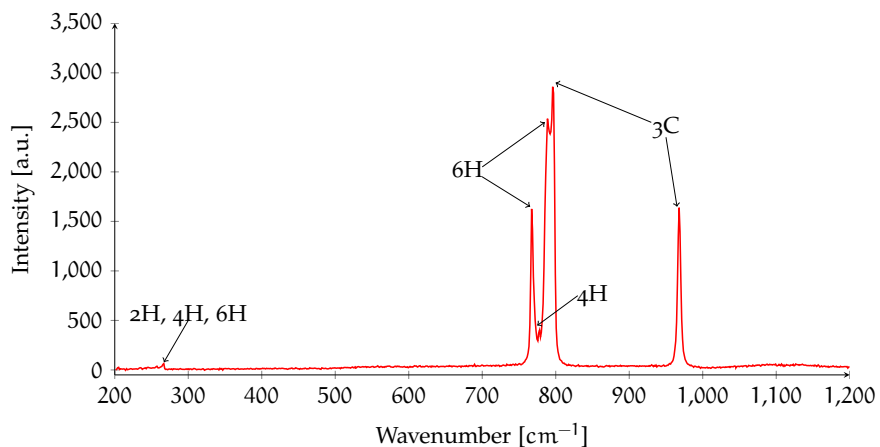


Figure 25: Raman Measurement of the sample ELS540 (1850°C) showing all Raman modes found on the sample giving the characteristic peaks for different polytypes like 4H-, 6H-, 3C- and 2H-SiC.

Using this additional information, given by the Raman measurement, the broad peak in the blue region from figure 24 comes from impurities built in to the other polytypes on the samples. The hexagonal polytypes feature a higher bandgap compared to the cubic one. For 6H-SiC the bandgap lies at 3eV, for 4H-SiC it lies at 3.2eV and for 2H-SiC it lies at 3.3eV as depicted in [7]. However, the probability of presence for 2H-SiC is quite low. Those bandgaps lead to a wavelength area from approximately 413nm to 375nm for a direct band to band tran-

sition. As already mentioned silicon carbide features an indirect bandgap. Therefore, the peak in figure 24 is not a band to band transition but a DAP. A reason for the introduction of donors and acceptors could be a contamination of the growth chamber by boron and aluminium from the source material and nitrogen from adsorbates at the growth setup parts, leading to co-doping of those polytypes [51].

By decreasing the temperature for the measurement of the photoluminescence spectrum, the probability of a band to band transition increases. Therefore, the characteristic peaks for the cubic polytype show up. Figure 26 shows the PL-spectrum of the sample ELS540 grown at 1850°C measured at 23K, 50K, 100°C and 150°C. Two peaks can be seen: One in the range of 450nm to 550nm and one in the range of 575nm to 650nm. Moreover, an increase of the intensity of the second peak can be seen by decreasing the temperature.

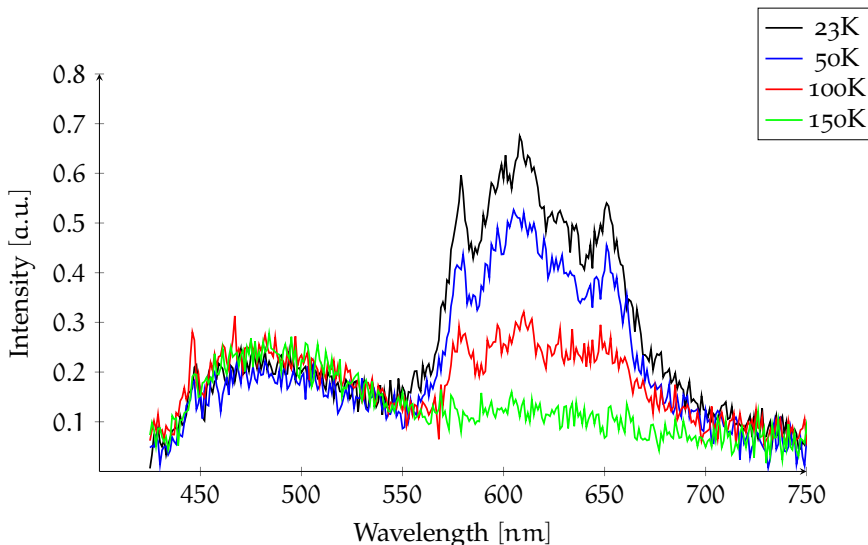


Figure 26: Temperature dependency of the PL-measurement for the sample ELS540 grown at 1850°C showing the increase of the intensity by decreasing the temperature down to 23K and no dependencies for the left peak.

The first peak, in the area of 490nm, which was assigned to DAP shows no dependencies to the change of temperature, supporting the statement that this luminescence is no consequence of exciton formation but a quasi-direct recombination from the substrate or the 4H-SiC/6H-SiC layer. The second peak however, shows a high dependency to the decrease of tem-

perature, which is typical for indirect bandgap semiconductors like β C-SiC. The band to band transition is getting quenched by phonons. With an increase of the temperature the phonon density increases and with that, the amount of non-radiative recombination.

With a further decrease in temperature down to 2K the characteristic exciton and phonon lines will appear in the PL-spectrum, which is a sign for the good quality of the measured material [18]. The optimal temperature to measure the bound excitons in SiC was found out to be between 1.3K and 2.1K, however this needs liquid helium to cool down the sample [22]. In different experiments it was found out that excitons in β C-SiC can either be trapped by impurities to form a nitrogen-bound-exciton complex, which subsequently decays by phonon and photon emission [60, 18, 22] or be free [30]. In both cases the typical peaks can only be obtained with low-temperature photoluminescence (LTPL). Figure 27 shows a spectrum of β C-SiC measured at LTPL, featuring the zero phonon line and its phonon replicas. The location of the zero phonon line shows an energy level of 3.79eV which is the exact same value presented by Yoshida [26](p. 453). This shows the presence of high quality β C-SiC without other polytypes in this measurement.

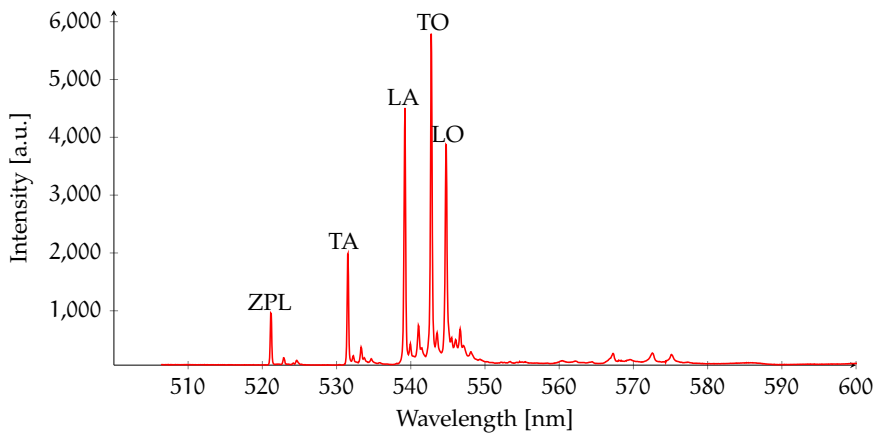


Figure 27: Photoluminescence spectrum of β C-SiC grown at 1900°C measured at 2K (LTPL) showing the Zero Phonon Line (ZPL) and the corresponding phonon replicas (TA, LA, TO and LO).

The exciton energy gap in β C-SiC was already determined to 2.390eV or 518.76nm as refered in [60]. The shift of the ZPL from this energy is approximately 10meV which agrees with other

works [60]. Those 10meV is supposed to be a measure of the binding between exciton and a neutral nitrogen in the system (four-particle complex). The four other peaks in figure 27 show the response of the phonon branches to the measurement at 2K for TA, LA, TO and LO. Table 6 shows the peak positions of the phonon branches substracted by the exciton binding energy 2.39eV and a comparison to values from references [60].

Table 6: Comparison of the measured energies for the phonon branches with reference values from literature and their variance [60]

Phonon branch	Measured	Reference	shift
ZPL	10.6meV	10meV	0.6meV
TA	57.2meV	46.3meV	10.9meV
LA	90.4meV	79.4meV	11meV
TO	105.6meV	94.4meV	11.2meV
LO	113.9meV	102.8meV	11.1meV

The values of the samples measured at 2K are showing a small shift of 10meV to the once from the reference which can be reasoned by either the temperature of the measurement in the reference work, which was 6K, the sensibility of the measurement equipment or the difference in thicknesses.

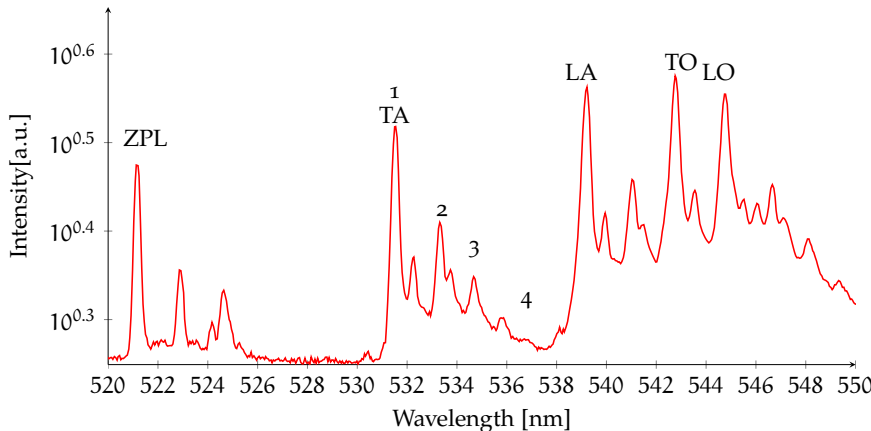


Figure 28: Photoluminescence spectrum of 2K measurement with a logarithmic intensity to show the peaks for the MBEC.

In [25] the origin of the additional emission lines between the phonon replica peaks were discussed and assigned to the emission of multiple bound exciton complexes (MBEC). The amount

of emission lines is equal to the number of bound electron-hole pairs bound to this complex. In figure 28 four additional lines can be accounted. The highest amount of emission lines observed was five [25]. The most common case of bound excitons in SiC is the tie to a neutral donor. In some cases more than one electron-hole pair can bind to this defect, leading to the MBEC, consisting of m holes and $m + 1$ electrons. During a recombination process one electron recombines with one hole leading to $m - 1$ holes and m electrons. The corresponding energy can either be transferred to a photon or to the remaining electrons at the donor. The result is an Auger process exciting the electron into the conduction band which is the dominant process [25].

To support the argument of the highest quality with the lowest temperature, which was stated in chapter 8, a PL-measurement of three samples grown at 1850°C , 1900°C and 1950°C was made at 77K . Figure 29 shows the results of those measurements close to the sample center. In this plot the spectral position of the two peaks is comparable to the ones in figure 26. The increase of DAP can be reasoned by an alignment problem.

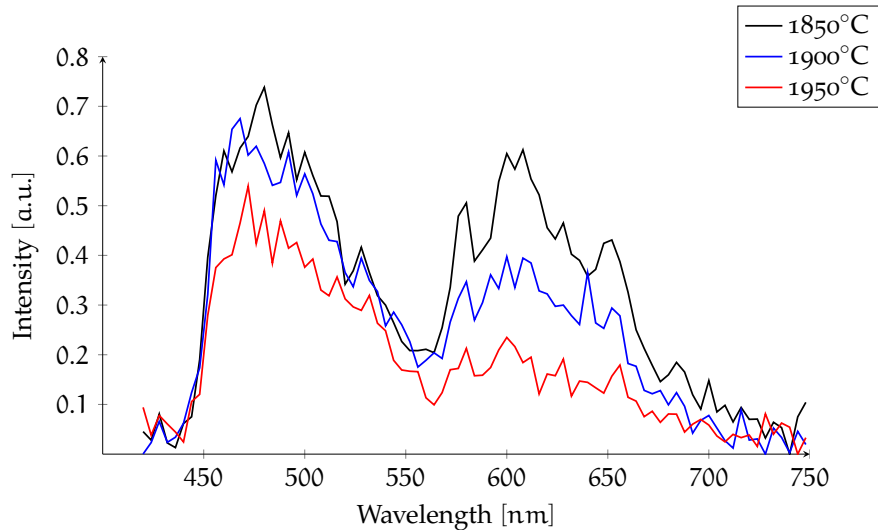


Figure 29: Intensity over wavelength for a photoluminescence measurement at 77K of the three samples grown at 1850°C , 1900°C and 1950°C showing two broad peaks: Left one corresponding to the other polytypes and their impurities and the right one showing the characteristic wavelength for $\beta\text{-SiC}$.

The characteristic β C-SiC peak on the right side however shows a relative increase compared to substrate DAP, supporting the assumption of higher quality for lower temperature, with the highest intensity for the sample grown at 1850°C and the lowest intensity for the sample grown at 1950°C .

To regard the effect of either the transition layer or the polytypes on the surface, a PL mapping from nucleation site in growth direction was made at 77K. Figure 30 shows the decrease of the luminescence while moving away from the nucleation site and the following increase of the DAP peak.

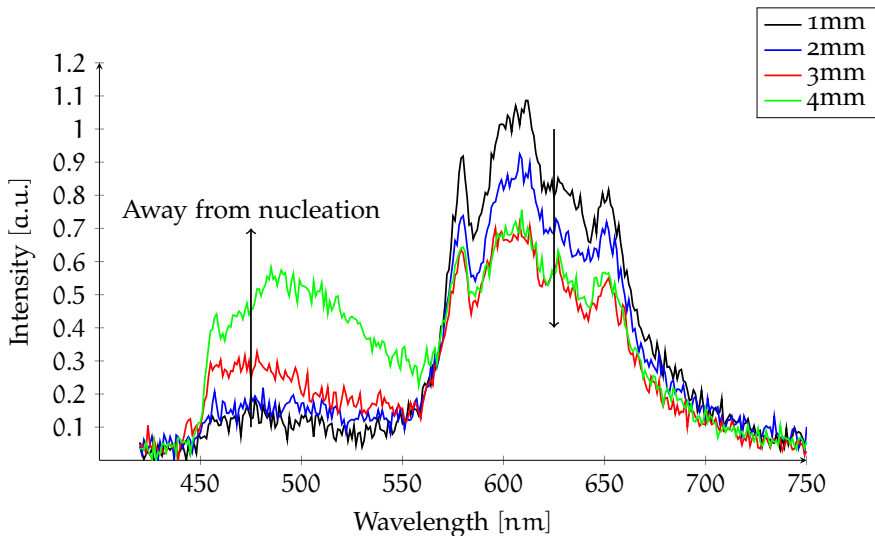


Figure 30: Measurement for a sample grown at 1850°C from nucleation side in step-flow direction, showing the increase of DAP and the decrease of intensity for the cubic system.

The results plotted in figure 30 show the response to the change of the layer thickness, due to the growth parameters.

To narrow down the correct reason for this effect a Raman mapping of the sample in growth direction was made. Figure 31 shows the results of this measurement. A clear change of the spectrum is visible by moving away from the nucleation site. New polytypes like 2H-, 4H- and 6H-SiC seem to emerge and introduce new Raman modes (fig. 25).

With those results, the first peak in the blue area can be assigned to the 4H-SiC transition layer co-doped with boron and nitrogen or 6H-SiC co-doped with aluminium and nitrogen. It

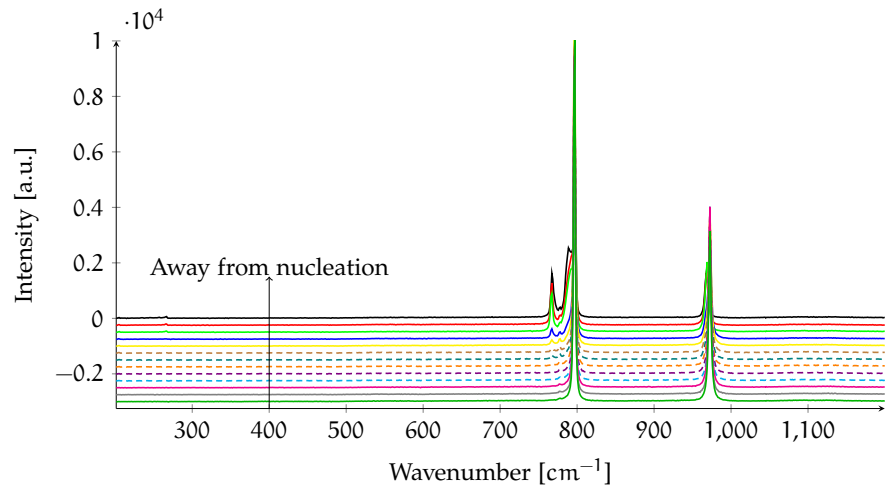


Figure 31: Raman Measurement of the sample ELS540 from the nucleation site in growth direction, showing peaks for 6H and 3C-SiC.

could also be reasoned by the 4H-SiC substrate.

The second peak — the characteristic peak for 3C-SiC — and its' decrease in growth direction can be reasoned by thinner 3C-SiC deposition (fig. 16).

In another measurement the cathodoluminescence (CL) setup was used on an undoped sample. In this method an electron beam instead of a laser with a higher energy was used. Therefore, a possible higher excitation density of the characteristic peaks is expected. Figure 32 shows the results of this CL measurement showing sharp peaks at around 550nm, 1100nm and 1650nm.

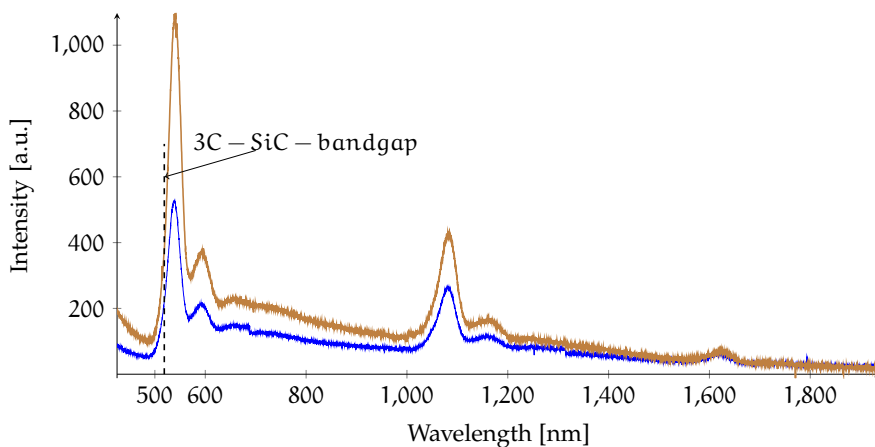


Figure 32: Cathodoluminescence measurement of an undoped sample grown at 1850°C for different positions, showing a sharp peak at 550nm and the corresponding diffractions at 1100nm and 1650nm from the material.

A reference measurement on a galliumarsenide sample showed no artificial anomalies on the CL-setup therefore the origin of the peaks at 538nm and 600nm comes from the sample. The resembling energy for those wavelenghts are 2.305eV and 2.07eV. The other peaks can be reasoned as second and third diffraction peaks of the first two. The DAP peak from the most likely 6H-, and 4H-SiC inclusions can barely be seen in the blue area left of the first peak, showing an intensity between 100a.u. and 200a.u.. The shift of approximately 0.33eV to 0.085eV from the bandgap can either be reasoned by an induced eletronic level by SFs or dislocations, or by variations in the measurement equipment [48]. The first effect was already suggested for n-doped 4H-SiC with an induced level, due to the SFs at 0.6eV below the conduction band, leading to a quantum well like defect reducing the total energy [48].

GROWTH RATE FOR BORON DOPED HOMOEPITAXIAL LAYER

This thesis also includes the growth of doped β C-SiC layers. For this approach a homoepitaxial growth using boron doped source material was implemented. The only changing factor for the experiments was the pressure to vary the mean free path and therefore the growth rate and incorporation of N_2 . The aimed thickness of the layers was around $300\mu m$ so the photoluminescence (PL) and the cathodoluminescence (CL) measurement could show an informative spectrum without an influence of other possible polytypes or contaminations on the seeds.

Figure 33 shows the linear decrease of the pressure for four of the five setups used. The fifth setup was the dynamic pressure were the atmosphere was kept at 10^{-4} mbar to 10^{-5} mbar.

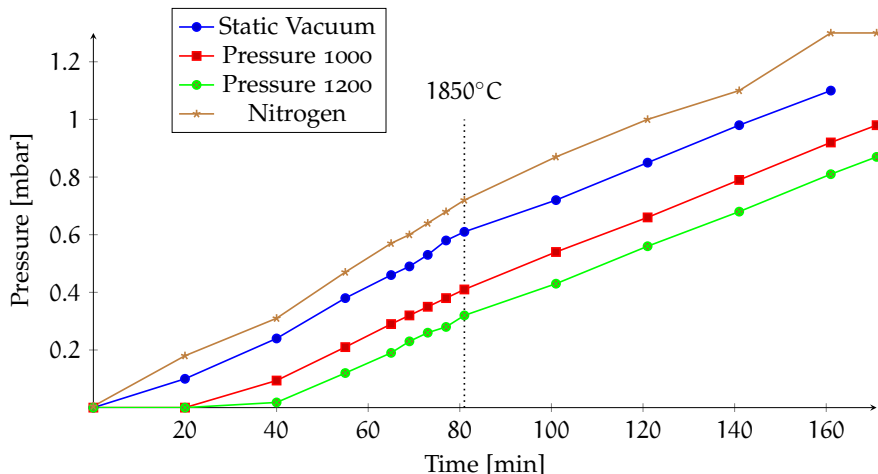


Figure 33: Evolution of the pressure over time during the growth process, due to leakage of the chamber system and a closed valve for the vacuum pump, and the starting point at $1850^\circ C$ for the actual growth.

Three of the shown setups vary in the time the valve for the turbo pump was closed. In the static vacuum the valve was closed right before the actual temperature ramp up began. The "Pressure 1000" and the "Pressure 1200" procedure had the moment of closure at a temperature of $1000^\circ C$ and $1200^\circ C$. The run in atmospheric pressure was done with a starting pressure

of 5×10^{-3} mbar.

Due to the leakage of the whole growth system a linear decrease in the pressure over time can be seen in all four setups but not in the run in the dynamic vacuum. The growth of all samples was realised at a temperature of 1850°C. At this temperature the nitrogen atmosphere showed the lowest pressure followed by the static vacuum, the "pressure 1000" and the "pressure 1200". It also has to be considered that the pressure increased during the whole growth for those four setups.

For a fast comparison of the grown sample quality, overview pictures of all as-grown doped layers were made. Figure 34 shows the result of thos micrographs.

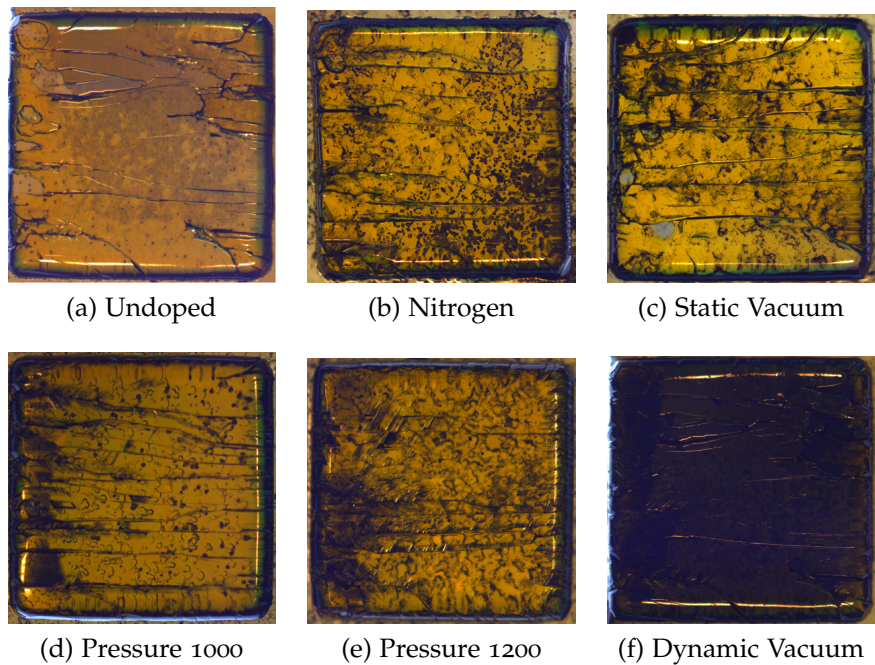


Figure 34: Overview pictures ($7 \times 7\text{ mm}^2$) of the as-grown doped layers with increasing growth rate from a to f and therefore, an expected increasee in the boron concentration leading to a higher absorbance of incoming light thus a darker appearance.

The first picture (a) shows an undoped 3C-SiC layer with some DPBs, as well as some polytype inclusions. This picture was included to show the change of color compared to the doped layers. Picture (b) shows the crystal layer grown in nitrogen

atmosphere. Most of the black dots in this frame can be reasoned by the back side sublimation, already mentioned in the heteroepitaxial growth section. However, the DPBs seem to become severe due to either the increase in thickness or due to the gathering of boron atoms. Figure (c) shows the sample grown in static vacuum. Like in picture (a) DPBs and some inclusions are visible. The backside sublimation is not so esential in this picture but existing. The lower row of figure 34 shows the samples grown in a higher pressure ambient from left to right. The sample grown at "pressure 1000" as well as the sample grown at "pressure 1200" do not show a big difference. However, a black area on the left side of the crystal can be observed leading to the assumption that the doping process also starts at the left side. Figure (f) shows one of two samples grown in dynamic vacuum featuring a dark surface.

The reason for the change of color from yellow/green to black is also reasoned by the increase of the growth rate with lower pressure. Figure 35 shows the growth rate for the different setups. The highest rate was observed for dynamic pressure with approximately $270 \frac{\mu\text{m}}{\text{h}}$ followed by "pressure 1200" and "pressure 1000". Static vacuum and the growth run in nitrogen atmosphere feature the lowest growth rate.

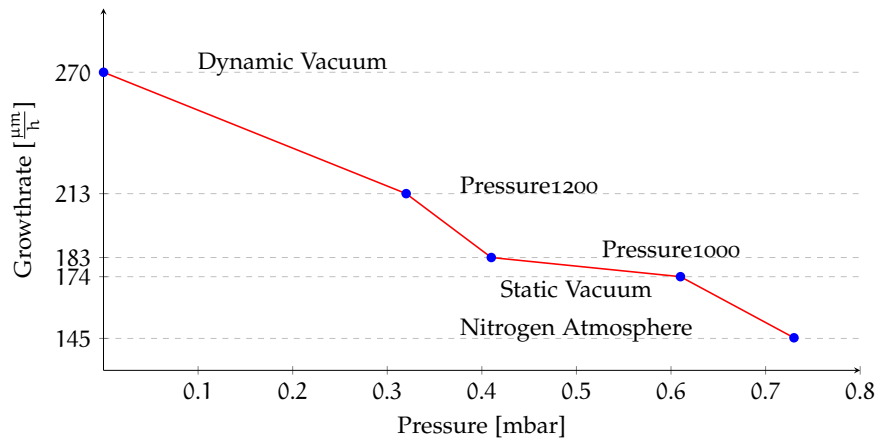


Figure 35: Plot of the growth rate over the pressure, showing the highest growth rate at the lowest pressure and a decrease with an increase of the pressure due to the change of the mean free path.

In equation 5 the dependencies for the mean free path were introduced. It shows a direct proportionality to the temperature

and an indirect proportionality to the pressure and the collision cross section σ . As the temperature is kept at 1850°C for the growth run and the temperature ramp up was the same for all setups ($20\frac{{}^{\circ}\text{C}}{\text{min}}$) the two influencing factors for the MFP are the pressure and σ .

In the case of undoped growth of $\beta\text{-SiC}$ the relevant gas species for the system were determined to N_2 , SiC_2 , Si_2C and Si . However, in the case of doped homoepitaxial layer growth the composition of the gas species is much more complex due to the addition of boron into the system. At the moment there is no possibility to determine the compositions, which makes it hard to calculate the influence on the MFP for those experiments. Nonetheless, the dependencies to the pressure and σ are still present leading to a decrease of the MFP with higher pressure and higher cross section collision.

PL-MEASUREMENT OF DOPED SAMPLES

The IBSC concept using boron doped β C-SiC can be initially tested using PL measurements. If the material exhibits an intermediate band related to boron and transitions to this level occur there should be peaks in PL spectrum around the following energies: $\text{VB} \rightarrow \text{B}(0.7\text{eV})$, $\text{B} \rightarrow \text{CB}(1.7\text{eV})$ and $\text{VB} \rightarrow \text{CB}(2.4\text{eV})$.

Figure 36 shows the sample ELS536 before the doping (a) and after the doping growth (b). The red circle shows the area the PL-measurement showed a peak for the characteristic β C-SiC.

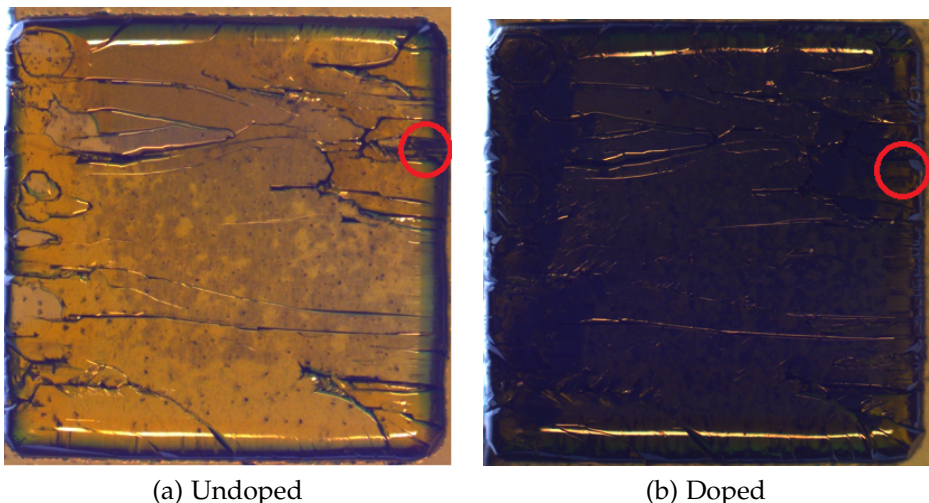


Figure 36: Overview pictures ($7 \times 7\text{mm}^2$) of the sample ELS536, showing the seeding crystal grown at 1950°C featuring some inclusions and DPBs(a) and the doped dark layer grown in dynamic vacuum (b). The red circle shows the area a PL measurement was made at different temperatures.

The sample was measured at different temperatures resulting the spectrum in figure 37 showing a broad peak in the range from 550nm to 750nm and a small peak in the blue region.

The high intensity for the measurement at 300K can be interpreted by an adjustment problem leading to a shift in the posi-

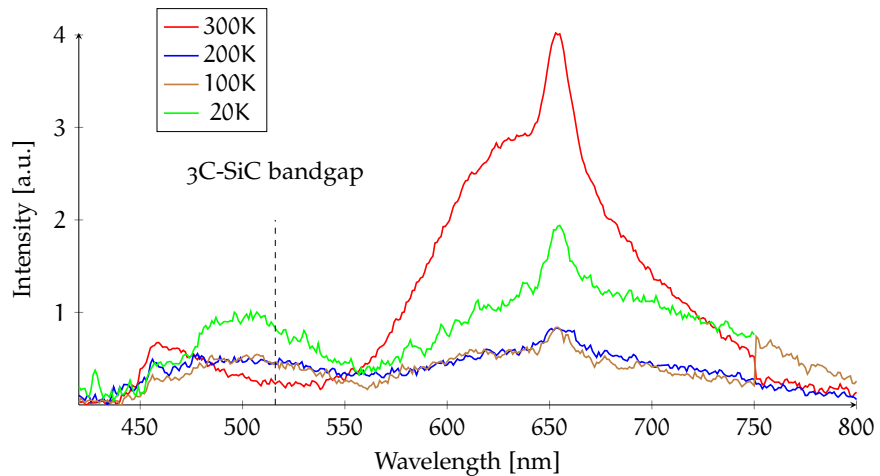


Figure 37: PL-spectrum of the doped ELS536 sample from the range of 425nm to 800nm measured at different temperatures and a 405nm laser showing a broad peak in the red/orange area and a small peak in the blue area.

tion. The measurement at 200K, 100K and 20K follow the trend already discussed in the chapter about the PL-spectrums for the seeding material.

In the next measurement another sensor was used to explore the region from 750nm to 1900nm. The excitation wavelenght of the laser was at 664nm. Figure 38 shows the spectrum for the sample ELS536 in this range with a sharp peak at 900nm, a broad peak from 950nm to approximately 1400nm and a sharp peak at 1328nm.

The first peak can be referred to the used glue to fixate the sample in the measurement system. The peak at 1328nm is reasoned by the laser as it is exactly twice the wavelenght of 664nm. The broad peak comes from defect related transitions since it is much below the bandgap of 3C-SiC.

The donor-acceptor pair luminescence is an effect which occurs in compensated semiconductors. This process describes a recombination of electrons with holes over donor and acceptor energy levels. In this case an intentional doping of boron and an unintentional doping of nitrogen and other contaminations occurred. To reach the limit of DAP the p-type doping of boron needs to be higher than the n-type doping, so the donor and acceptor impurities are compensated. During an excitation process —like PL-measurement— charge carriers (electrons or

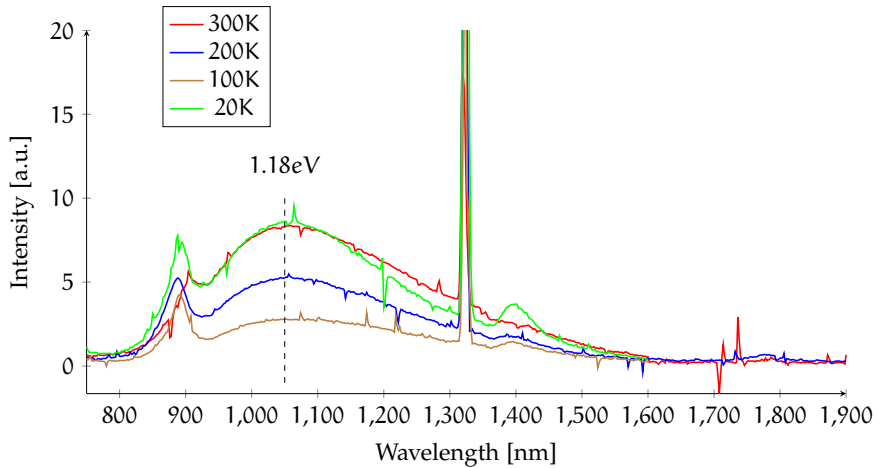


Figure 38: PL-spectrum of the doped ELS536 sample from the range of 750nm to 1900nm measured at different temperatures and a 664nm laser showing a first peak around 900nm reasoned by the glue to fixate the sample, a second broad peak from 950nm to 1400nm, which is equivalent to an energy level of 1.305eV to 0.886eV and the laser at 1328nm.

holes) can be trapped forming neutral donors and neutral acceptors. Those will eventually pair and form the donor-acceptor pair excitons which can efficiently luminesce [62].

In the PL spectrum no clear sign of an intermediate band at the positions 1550nm and 827nm is visible. However, the measurement shows a broad DAP peak in the β C-SiC from 900nm to 1400nm. The broad peak comes from many different energetic defects in the range of 1.37eV to 0.8eV.

Part V

CONCLUSION

CONCLUSION

Heteroepitaxial growth of β C-SiC seeding material on 4° off-axis 4H-SiC substrates and homoepitaxial growth of boron doped layers on β C-SiC seeds as a future solar cell material was explored in this work using the sublimation epitaxy approach. The purpose of this work was to produce an IBSC. But, no intermediate band was observed by PL measurements, but a DAP in the range of 950nm to 1400nm was visible.

Furthermore, an investigation of the seeding material was made using optical microscopy, PL, Raman and KOH-etching. A correlation between the growth rate and the amount of DPBs was observed, showing a lower amount of boundaries with lower growth rate. By etching as-grown samples in KOH it was possible to reveal the SFs and evaluating them using analysis software and OM. An increase of the SF density in growth direction was observed, leading to the assumption of a decrease with higher thickness due to the decrease of thickness in growth direction (fig. 16). The use of LTPL measurements revealed high quality of the β C-SiC layer further PL and Raman measurements show a need for thick samples ($> 1\text{mm}$) to accomplish e.g. bulk growth and an inclusion (6H-SiC and 4H-SiC) and defect-free (SFs and dislocation lines) seeding crystal. The different pressure setups during the doping process were not compared. Therefore, the one sample with the highest expected doping concentration was evaluated ("dynamic vacuum"). This sample did not show an intermediate band but a DAP which can be assigned to the β C-SiC material was observed.

In order to obtain an intermediate band a higher doping concentration is needed in the layer. Therefore, a higher doped source material and further investigation on the different parameters in this setup are needed (pressure, ramp-up, growth rate, growth temperature).

BIBLIOGRAPHY

- [1] A. Martí A. Luque. Increasing the efficiency of ideal solar cells by photon induced transitions at intermediate levels. *Physical Review Letters*, 78:26, 1997.
- [2] P. G. Linares I. Ramiro I. Artacho E. López E. Hernández M. J. Mendes A. Mellor I. Tobías D. F. Marrón C. Tablero A. B. Cristóbal C. G. Bailey M. Gonzalez M. Yakes M. P. Lumb R. Walters A. Luque A. Martí, E. Antolín. Six not-so-easy pieces in intermediate band solar cell research. *Journal of Photonics for Energy*, 3:031299–1, 2013.
- [3] M. Camarda N. Piluso F. La Via A. Severino, R. Anzalone. Structural characterization of heteroepitaxial β c-sic. *Materials Science Forum*, 711:27–30, 2012.
- [4] SiCrystal AG. Production specification. Technical report, Thurn-und-Thaxis-Stra. 20 90411 Nuremberg, Germany.
- [5] W.C. Mitchel H. M. Hobgood A.O.Evwaraye, S. R. Smith. Boron acceptor levels in 6h-sic bulk samples. *Applied Physics Letters*, 71.9:1186–1188, 1997.
- [6] R. P. Corkish C. A. Zorman M. Mehregany M. Ioescu M. A. Green B. S. Richards, A. Lambertz. β c-sic as a future photovoltaic material. In *3rd World Conference on Photovoltaic Energy Conversion*, 2003.
- [7] U. Lindefelt C. Persson. Detailed band structure for β c-, 2h-, 4h-, 6h-sic, and si around the fundamental band gap. *Physical Review B*, 54:15, 1996.
- [8] G. Muziol M. Siekacz M. Sawicka G. Cywiński Z. R. Wasilewski S. Porowski C. Skierbiszewski, H. Turski. Nitride-based laser diodes grown by plasma-assisted molecular beam epitaxy. *Journal of Physics D: Applied Physics*, 47:073001, 2014.
- [9] Po-Hsun Chen. Stability of bulkcubic silicon carbide (β c-sic)on off orientedhexagonal silicon (4h-sic) substrate. Master's thesis, University of Linköping, 2013.

- [10] An-Sheng Cheng. Study of 3c and 6h sic polytype stability in sublimation epitaxial growth using on-axis substrates. Master's thesis, University of Linköping, 2012.
- [11] W. J. Choyke. The physics and chemistry of carbides, nitrides, and borides. *NATO ASI Series E: Applied Sciences*, 185:853, 1990.
- [12] M. Pons D: Chaussende, P. J. Wellmann. Status of sic bulk growth processes. *Journal of Physics D: Applied Physics*, 40: 6150–6158, 2007.
- [13] J. A. Powell L. G. Matus D. J. Larkin, P. G. Neudeck. Site-competition epitaxy for controlled doping of cvd silicon carbide. *Institute of Physics Conf.*, 137:51–54, 1994.
- [14] T. Hölzel A.Wohlfart D. Siche, D. Klimm. Reproducible defect etching of sic single crystals. *Journal of Crystal Growth*, 270:1–6, 2004.
- [15] J. H. Edgar D. Zhuang. Wet etching of gan, aln, and sic: a review. *Mat. Science Eng.*, R 48.1:1–46, 2005.
- [16] R. F. Davis. Glass, in advances in solid state chemistry. *JAI, Greenwich, CT*, 2:1–111, 1991.
- [17] A.Belabbes F. Bechstedt. Structure, energetics and electronic states of iii-v compound polytypes. *Journal of Physics: Condensed Matter*, 25:273201, 2013.
- [18] Z. C. Feng. Optical properties of cubic sic grown on si substrate by chemical vapor deposition. *Microelectronic Engineering*, 83:165–169, 2006.
- [19] A. Fissel. Thermodynamic considerations of the epitaxial growth of sic polytypes. *Journal of Crystal Growth*, 212:438–450, 2000.
- [20] M. J. Keevers R. Corkish M. A. Green G. Beaucarne, A. S. Brown. The impurity photovoltaic (ipv) effect in wide-bandgap semiconductors: an opportunity for very-high-efficiency solar cells? *Progress in Photovoltaics: Research and Applications*, 10:345–353, 2002.
- [21] Prasad M. Dudley G. Dhanaraj, K. V. Byrappa. *Springer Handbook of Crystal Growth*. Springer, 2010.

- [22] W. J. Choyke G. Pensl. Electrical and optical characterization of sic. *Physica B*, 185:264–283, 1993.
- [23] S. Öberg P. R. Briddon H. Iwata, U. Lindefelt. Theoretical study of planar defects in silicon carbide. *Journal of Physics: Condensed Matter*, 14:12733–12740, 2002.
- [24] ADMAP Inc. Prodction specification. Technical report, Mitsui Source, Tokyo.
- [25] W. J. Choyke J. P. Bergman E. Janzén. Multiple bound exciton associated with the nitrogen donor in 3c silicon carbide. *phys. stat. sol.*, 210:407–412, 1998.
- [26] Yukinobu Kumashiro. *Electric Refractory Materials*. Marcel Dekker, Inc., 2000.
- [27] D. J. Larkin. Sic dopant incorporation control using site-competition cvd. *Phys. Status Solidi, B* 202.1:305–320, 1997.
- [28] A. Lebedev. Deep level centers in silicon carbide: A review. *Semiconductors*, 33:107–130, 1999.
- [29] R. Azevedo M. B. J. Wijesundara. *Silicon Carbide Microsystems for Harsh Environments*. Springer New York, 2011.
- [30] H. Matsunami M. Ikeda. Free exciton luminescence in 3c, 4h, 6h, and 15r sic. *phys. stat. sol.*, 58:657, 1980.
- [31] M. A. Green M. J. Keevers. Efficiency improvements of silicon solar cells by the impurity photovoltaic effect. *Journal of Applied Physics*, 75:4022, 1994.
- [32] V. Jokubavicus S. Schimmel M. Syväjärvi Y. Ou H. Ou M. K. Linnarsson P. Wellmann M. Kaiser, T. Hupfer. Polycrystalline sic as source material for the growth of fluorescent sic layers. *Materials Science Forum*, 740-742:39–42, 2013.
- [33] E. Johansson A. Henry Q. Wahab C. Hallin E. Janzén M. Syväjärvi, R. Yakimova. Purity and surface structure of thick 6h and 4h sic layers grown by sublimation epitaxy. *Material Science Eng., B* 61-62.0:147–150, 1999.
- [34] H. Jacobsson E. Janzén M. Syväjärvi, R. Yakimova. Growth of 3c-sic using off-oriented 6h-sic substrates. *Materials Science Forum*, 353-356:143–146, 2001.

- [35] M. Tuominen A. Kakanakova-Georgieva M. Macmillan A. Henry Q. Wahab E. Janzén M. Syväjärvi, R. Yakimova. Growth of 6h and 4h-sic by sublimation epitaxy. *Journal of Crystal Growth*, 197.1-2:155–162, 1999.
- [36] R. Yakimova M. Syväjärvi, N. Sritirawisarn. Initial growth in 3c-sic sublimation epitaxy on 6h-sic. *Materials Science Forum*, 556-557:195–198, 2007.
- [37] S. G. Müller. *Herstellung von Siliziumkarbid im Sublimationsverfahren*. PhD thesis, Friedirch-Alexander University erlangen-Nuremberg, 1998.
- [38] D. J. Spry J. A. Powell H. Du M. Skowronski X. R. Huang M. Dudley P. G. Neudeck, A. J. Trunek. Cvd growth of 3c-sic on 4h/6h mesas. *Chemical Vapor Deposition*, 12:531–540, 2006.
- [39] F. Oehlschläger P. Wellmann R. Yakimova P. Hens, M. Syväjärvi. P- and n-type doping in sic sublimation epitaxy using highly doped substrates. *Material Science Forum*, 615 - 517:85–88, 2009.
- [40] L. Kadinski M. Selder T. L. Straubinger A. Winnacker P. J. Wellmann, D. Hofmann. Impact of source material on silicon carbide vapor transport growth process. *Journal of Crystal Growth*, 225:312–316, 2001.
- [41] F. Bechstedt P. Käckell, J. Furthmüller. Stacking faults in group-iv crystals: An ab initio study. *Physical Review B*, 58: 1326–1330, 1998.
- [42] F. Tournus A. Perez P. Melinon, B. Masenelli. Playing with carbon and silicon at the nanoscale. *Nature Materials*, 6: 479–490, 2007.
- [43] M. Beshkova R. Yakimova R. Vasiliauskas, M. Syväjärvi. Two-dimensional nucleation of cubic and 6h silicon carbide. *Materials Science Forum*, 615-617:189–192, 2009.
- [44] P. Hens P. Wellmann M.I Syväjärvi R. Yakimova R. Vasiliauskas, M. Marinova. Nucleation control of cubic silicon carbide on 6h- substrates. *Crystal Growth & Design*, 12:197–204, 2012.
- [45] N. Sritirawisarn M. Syväjärvi R. Yakimova, G. R. Yazdi. Structure evolution of 3c-sic on cubic and hexagonal substrates. *Materials Science Forum*, 527-529:283–286, 2006.

- [46] E. Janzén R. Yakimova M. Syväjärvi. Wetting properties and interfacial energies in liquid phase growth of α -sic. *Material Science Forum*, 264-268:159–162, 1998.
- [47] Dominik Rankl. Nukleation von kubischem sic bei der sublimationsepitaxie. Master's thesis, Friedrich-Alexander University Erlangen-Nuremberg, 2013.
- [48] P. Hens R. Müller D. Queren U. Kunecke K. Konias R. Hock A. Magerl M. Pons A. Winnacker P. Wellmann S. A. Sakwe, M. Stockmeier. Bulk growth of sic - review on advances of sic vapor growth for improved doping and systematic study on dislocation evolution. *phys. stat. sol.*, 245:1239–1256, 2008.
- [49] D. Hofmann L. Kadinski P. Kaufmann M. Kölbl E. Schmitt S. G. Müller, R. Eckstein. Modelling of the pvt-sic bulk growth process taking into account global heat transfer, mass transport and heat of crystallization and results on its experimental verification. *Material Science Forum*, 364-268:57–60, 1998.
- [50] R. P. Devaty w. J. Choyke D. J. Darkin H. S. Kong T. Troffer G. Pensl S. G. Sridhara, L. L. Clemen. Photoluminescence and transport studies of boron in 4h sic. *Journal of Applied Physics*, 83:7909–7919, 1998.
- [51] Saskia Schimmel. Growth and doping of fluorescent 6h-sic layers. Master's thesis, Friedrich-Alexander University Erlangen-Nuremberg, 2012.
- [52] W. Sutherland. Lii. the viscosity of gases and molecular force. *Philosophical Magazine Series 5*, 36:507–531, 1893.
- [53] M. Syväjärvi. *Comprehensive Semiconductor Science and Technology, Sublimation Epitaxial Growth of Hexagonal and Cubic SiC*. Elsevier: 202–231, 2011.
- [54] M. Kaiser V. Jokubavicius M. Syväjärvi P. J. Wellmann T. Hupfer, P. Hens. Modeling of the mass transport during the homo-epitaxial growth of silicon carbide by fast sublimation epitaxy. *Materials Science Forum*, 740-742:52–55, 2013.
- [55] S. Öberg P. R. Briddon U. Lindefeld, H. Iwata. Stacking faults in 3c-, 4h-, and 6h-sic polytypes investigated by an

- ab initiosupercell method. *Physical Review B*, 67:155204, 2003.
- [56] R. Liljedahl J. W. Sun M. Kaiser P. Wellmann S. Sano R. Yakimova S. Kamiyama M. Sjväjärvi V. Jokubavicius, P. Hens. Effect of source material on epitaxial growth of fluorescent sic. *Thin Solid Films*, 522:7–10, 2012.
- [57] R. Yakimova M. Syväjärvi V. Jokubavicius, P. Chen. Lateral enlargement of 3c-sic on off-oriented 4h-sic substrates. In *The Department of Physics, Chemistry and Biology (IFM) Linköping University*, volume Linköping, 2013.
- [58] S. Schimmel R. Liljedahl R. Yakimova M. Syväjärvi V. Jokubavicius, H. Huang. Towards bulk-like 3c-sic growth using low off-axis substrates. *Materials Science Forum*, 740-742:275–278, 2013.
- [59] R. Vasiliauskas. *Sublimation Growth and Performance of Cubic Silicon Carbide*. PhD thesis, Linköping University, 2012.
- [60] L. Patrick W. J. Choyke, D. R. Hamilton. Optical properties of cubic sic: Luminescence of nitrogen-exciton complexes, and interband absorption. *Physical Review*, 133:4a, 1964.
- [61] J Queisser W. Shockley, H. Detailed balance limit of efficiency of p-n junction solar cells. *Journal of Applied Physics*, 32:510–519, 1961.
- [62] F. Williams. Donor-acceptor pairs in semiconductors. *Phys. Status Solidi*, 25:493, 1968.
- [63] M. G. Ramm A. D. Roenkov Y. A. Vodakov, E. N. Mokhov. Epitaxial growth of silicon carbide layers by sublimation sandwich method (i) growth kinetics in vacuum. *Crystall Research& and Technology*, 14:729–740, 2006.
- [64] M. G. Ramm E. N. Mokhov Y. N. Makarov Y. A. Vodakov, A. D. Roenkov. Use of ta-container for sublimation growth and doping of sic bulk crystals and epitaxial layers. *phys. stat. sol.*, 202:177, 1997.

DECLARATION

I hereby declare that this thesis is my own work and has not been submitted in any form for another degree or diploma at any university or other institute of tertiary education. All information derived from the published and unpublished work of others is referenced.

Ich versichere, dass ich die Arbeit ohne fremde Hilfe und ohne Benutzung anderer als der angegebenen Quellen angefertigt habe und dass die Arbeit in gleicher oder ähnlicher Form noch keiner anderen Prüfungsbehörde vorgelegen hat und von dieser als Teil einer Prüfungsleistung angenommen wurde. Alle Ausführungen, die wörtlich oder sinngemäß übernommen wurden, sind als solche gekennzeichnet.

Linköping, September 16, 2014

Philipp Schuh, September
16, 2014